

Inhibitive Chain Transfer to Ligand in the ATRP of *n*-Butyl Acrylate

Rahul Sharma, Ayush Goyal, James M. Caruthers, and You-Yeon Won*

School of Chemical Engineering, Purdue University, West Lafayette, Indiana 47907

Received February 20, 2006; Revised Manuscript Received May 5, 2006

ABSTRACT: The *N,N,N',N',N''*-pentamethyldiethylenetriamine (PMDETA) ligand, commonly used in copper-catalyzed atom transfer radical polymerization (ATRP), is known to have an inhibitive effect on the kinetics of the ATRP of alkyl acrylate monomers due to the chain transfer reaction involving the ligand species. However, the exact chemical nature of the ligand radicals resulting from the chain transfer reaction and other reactions that the ligand radicals may undergo subsequently are presently unknown, making it difficult to establish the precise reaction mechanism of the copper/PMDETA-based ATRP of alkyl acrylate monomers. In an effort to gain a better understanding of the chemistries and reactions of the PMDETA species in the ATRP of *n*-butyl acrylate, we conducted (i) experimental measurements to determine how changes in PMDETA concentration influence the ATRP kinetics and the molecular properties of the product, (ii) electron density functional theory (DFT) calculations to identify probable pathways for reactions involving the PMDETA ligand, and (iii) fitting of the experimental data obtained from (i) to a kinetic model derived on the basis of the reaction feasibility analyses from (ii) to test the validity of the proposed ATRP mechanism. The results suggest that (a) the proton abstraction from the PMDETA ligand occurs predominantly at a specific site of the molecule, (b) once generated, the ligand radical is unlikely to be involved in any further reaction, and (c) there appears to exist a disparity in the reactivity of PMDETA toward chain transfer reactions between the free and copper-bound states.

1. Introduction

Atom transfer radical polymerization (ATRP) involves an equilibrium between dormant (halide-terminated) and active (radical) species that is typically heavily biased toward the inactivated state of the growing polymer species, enabling the effectively termination-free addition of monomers to the ends of growing chains.^{1,2} The transformation between the dormant species and active radical is catalyzed through a reversible halide transfer between the growing chain and a transition metal (such as copper) which undergoes the corresponding change in its oxidation state.^{3,4} By far the most common ATRP reactions are performed utilizing monomers themselves or with added organic solvent as the reaction medium, and the use of such nonpolar reaction media necessitates the complexation of the transition metal catalyst with a ligand molecule in order to ensure sufficient solubilization of the catalyst in the reaction mixture. Nitrogen-based ligands have been most commonly used, for instance, in copper-based ATRP,² and the two common types of nitrogen ligands are (i) aromatic compounds containing sp²-hybridized nitrogen atoms available in the form of R₁=N–R₂ (such as 2,2'-bipyridine and 4,4'-di(5-nonyl)-2,2'-bipyridine) and (ii) aliphatic substances containing sp³ nitrogens in the form of R₁–NR₂–R₃ (such as *N,N,N',N',N''*-pentamethyldiethylenetriamine (PMDETA) and *N,N,N',N',N'',N''*-hexamethyltriethyltetramine).⁵ Compared to their aliphatic counterparts, aromatic N-based ligands in general allow better solubilization of the transition metal salt in the low-dielectric organic solvent (likely due to the bulkier nonpolar moieties), and they usually induce a higher oxidation potential of the complexed metal center, leading to a greater tendency toward radical deactivation in the atom transfer equilibrium and therefore slower overall polymerization rates.^{6–8} Mainly because of the advantage of achieving a faster polymerization without causing any significant broadening of the molecular weight distribution of the product, aliphatic nitrogen ligands such as PMDETA have been more frequently

adopted over the aromatic ligands for synthesis of model polymers using ATRP.

The roles that the ligand molecules play in the ATRP chemistry were originally believed to be limited to the solubilization of the transition metal and the adaptation of the redox potential of the metal catalyst for ATRP without explicitly participating in the ATRP reactions.² Recently, experimental evidence has emerged that a chain transfer reaction (which involves the transfer of a proton from some species to the active chain) exists in the ATRP of alkyl acrylate monomers using the PMDETA ligand; Kubisa and co-workers' matrix-assisted laser desorption/ionization time-of-flight (MALDI-TOF) mass spectroscopy analyses of the ATRP-synthesized poly(*tert*-butyl acrylate) (PtBA) showed that the bromide(Br)-terminated dormant PtBA chains are gradually converted to H-terminated nonpropagatable (dead) PtBA chains with the progress of the ATRP reaction to a degree that cannot be explained by the conventional four-component (i.e., initiation, equilibrium, propagation, and termination) ATRP reaction mechanism.⁹ Regarding the preferred mechanism for the observed chain transfer, different explanations have been proposed; on the basis of combined gel permeation chromatography (GPC) and viscosity measurements on the ATRP-prepared poly(butyl acrylate), it has been suggested that the radical is likely transferred to a polymer;¹⁰ however, this tentative explanation contradicted further MALDI-TOF examination of low molecular weight poly(alkyl acrylate) polymers prepared using the PMDETA-based ATRP techniques, which did not detect any branched polymer product (which would contain more than one bromide atoms per chain), leading to a more convincing speculation that chain transfer to PMDETA occurs in the ATRP of alkyl acrylate monomers.¹¹ The occurrence of chain transfer to the ligand has been further supported more recently by kinetic experiments performed by Matyjaszewski and co-workers that demonstrate increased retardation of polymerization with increasing PMDETA concentration in the bulk homogeneous ATRP of *n*-butyl acrylate (nBA).¹²

* To whom correspondence should be addressed. E-mail: yywon@ecn.purdue.edu.

Although the previous MALDI-TOF results unambiguously establish that the radical transfer to the PMDETA ligand yields an inactive ligand product that does not reinitiate chains,¹¹ the exact chemical nature of the ligand product and its fate for the remaining period of polymerization remain unexplored. Detailed understanding of the chemistries and reactions that the species produced by the ligand transfer reaction would entail is an important missing element in incorporating the ligand transfer phenomenon into the overall mechanism of the ATRP of *n*BA and thus in establishing a polymerization reaction model for predicting the product properties (such as average molecular weights and molecular weight distributions) in relation to the polymerization conditions. In this report, we discuss the mechanistic details concerning the overall inhibitive effects of PMDETA on the kinetics of the ATRP of *n*BA and also regarding the likely fate of the ligand species that results from the transfer reaction. For this purpose, we take a threefold approach consisting of (i) experimental investigation of the kinetics of the ATRP of *n*BA (to collect information about how changes in PMDETA concentration impact the ATRP kinetics and the product properties such as molecular weight distribution), (ii) electron density functional theory (DFT) calculations using established computational methodologies (for identifying thermodynamically most probable pathways for possible side reactions involving the PMDETA ligand), and (iii) fitting of the experimental kinetic and property data from (i) using a mechanistic model formulated on the basis of the reaction feasibility analyses from (ii) (to determine the validity of the proposed ATRP mechanism). As a result of studies covering a wide range of possible reaction scenarios, we present a mechanism for the PMDETA-based ATRP of *n*BA that satisfies consistency between the experimental data and the kinetic model derived from the proposed reaction mechanism. The validity of the proposed mechanism is also supported by the reasonableness of the kinetic rate constants obtained from the kinetic data fitting in comparison to the reported values for the corresponding rate constants available in the literature, and also the best-fit rate constants estimated from the kinetic modeling are capable of reasonably reproducing the polydispersity data as functions of polymerization conditions without any further adjustment of their values. This work was conducted as part of our project to develop a kinetic model that can be utilized as a predictive tool for determining the molecular characteristics of ATRP-synthesized poly(*n*-butyl acrylate)-based block copolymers, and all polymerization kinetic measurements were implemented using a bromopropionate-end-functionalized poly(ethylene oxide) (PEO) as a macroinitiator.

2. Methods and Procedures

2.1. Materials and Characterization. Poly(ethylene oxide) monomethyl ether (PEO-ME, M_n (number-average molecular weight) = 5000 g/mol, M_w (weight-average molecular weight) = 5400 g/mol) was purchased from Polysciences, Inc. *n*-Butyl acrylate (*n*BA, 99% purity, Aldrich) was first purified with calcium hydride (CaH_2) at room temperature overnight and then distilled and stored over molecular sieves of pore size 4 Å at 4 °C before use. Copper(I) bromide (Cu(I)Br , 99.999% purity, Aldrich) was purified by stirring in galacial acetic acid, followed by washing with ethanol and diethyl ether. After drying under vacuum, it was stored under a nitrogen atmosphere before use. Anhydrous dichloromethane (99.8% purity) and *N,N*-dimethylformamide (DMF, 99.8% purity) were purchased from Sigma-Aldrich and stored over molecular sieves before use. *N,N,N',N',N'*-Pentamethyldiethylenetriamine (PMDETA, 99% purity, Aldrich) was stored over KOH before use. Triethylamine (TEA, 99% purity) and 2-bromopropionyl chloride (BPC, technical grade) were purchased from Sigma-Aldrich and

used as received. All other chemical reagents were used without further purification after purchase.

¹H NMR (300 MHz) spectroscopy measurements were performed using a Bruker ARX300 spectrometer available at the Purdue Interdepartmental NMR Facility, and all NMR spectra were taken at room temperature from ca. 0.1% (w/w) polymer solutions in CDCl_3 . GPC measurements were carried out using a Water Breeze HPLC system consisting of an HPLC pump, two Phenogel columns of 0.4 and 0.05 μm pore sizes, and a differential refractometer. Tetrahydrofuran (THF) was used as the eluent at a flow rate of 1 mL/min at 30 °C. The correlation between the elution time and the polymer molecular weight was predetermined using polystyrene molecular weight standards.

2.2. Polymer Synthesis. PEO Macroinitiator Preparation. PEO-ME (25 g, 5 mmol) was weighed and charged to a 500 mL round-bottom flask. The flask was sealed with a rubber septum and cycled thrice between vacuum and nitrogen at room temperature. The polymer was then heated at 110 °C under vacuum for 1 h to remove trace water. After cooling the flask to room temperature under nitrogen, dichloromethane (75 mL) was added via syringe to dissolve the polymer. The solution was then placed in an ice bath, and TEA (0.7 mL, 5 mmol) was added to the polymer solution. Finally, BPC (1.31 mL, 12.5 mmol) was added dropwise over a period of 1 h. The ice bath was then removed, and the end-functionalization reaction was allowed to proceed for 24 h at room temperature.

After completion of the reaction, the suspension was filtered to remove all insolubles, and the resultant macroinitiator was precipitated by adding large excess of diethyl ether (technical grade) to the filtrate. The macroinitiator was isolated by filtration and washed with diethyl ether. After recrystallization from ethanol (technical grade), the product was washed again with diethyl ether and then dried under vacuum at room temperature for a day. The final product, a white crystalline powder weighing ~21 g (84% yield), was stored under a nitrogen atmosphere.

Parts a and b of Figure 1 present ¹H NMR spectra of the PEO-ME precursor and the PEO macroinitiator, respectively. The complete bromopropionyl end-functionalization of PEO-ME (i.e., ~99.3%) was confirmed by the ratio of the area under the peak at $\delta = 1.9$ ppm that corresponds to proton "d" defined in Figure 1b to the area under the peak at $\delta = 3.6$ ppm corresponding to the backbone $-\text{CH}_2-$ protons of PEO (proton "a" in Figure 1b).

ATRP of *n*BA. The insolubility of the $\text{Cu(II)Br}_2/\text{PMDETA}$ complex in pure *n*BA causes the reaction system to become heterogeneous in the bulk ATRP of *n*BA. The heterogeneous polymerization typically involves many complicating factors that defy precise modeling of the process. For this reason, we opted to conduct the ATRP kinetic experiments under homogeneous condition, and following the procedure of Matyjaszewski and co-workers,¹² we used DMF as cosolvent, typically added at 10 vol % of the monomer, to achieve complete solubilization of the $\text{Cu(II)Br}_2/\text{PMDETA}$ catalyst complex.

Immediately prior to use, PEO macroinitiator (1.25 g, 0.25 mmol) was dried under vacuum at 90 °C for 4 h. It was then dissolved in a mixture of *n*BA (4 mL) and DMF (0.25 mL) at 90 °C. In another flask, Cu(I)Br (36 mg, 0.25 mmol) was dispersed in *n*BA (1 mL) with added DMF (0.25 mL) at 90 °C, and a desired amount of PMDETA was added to the mixture. After stirring for 30 min, the catalyst solution was transferred through a cannula to the macroinitiator solution in order to trigger the initiation. Small-amount samples were withdrawn at regular intervals of time using a gastight syringe and immediately immersed in liquid nitrogen to quench the reaction. After allowing the samples to attain room temperature, they were dissolved in dichloromethane, and the copper catalyst was removed by liquid-liquid extraction using water as the extractant. The catalyst-free polymer was then dried at 100 °C under vacuum for 12 h.

Figure 1c illustrates a typical ¹H NMR spectrum of PEO-PnBA diblock copolymer. The signals appearing at 1.9 ppm (position "c" in Figure 1c), 2.3 ppm ("e"), 4.0 ppm ("d"), 1.6 ppm ("f"), 1.4 ppm ("b"), and 0.9 ppm ("g") confirm the PnBA block. The block

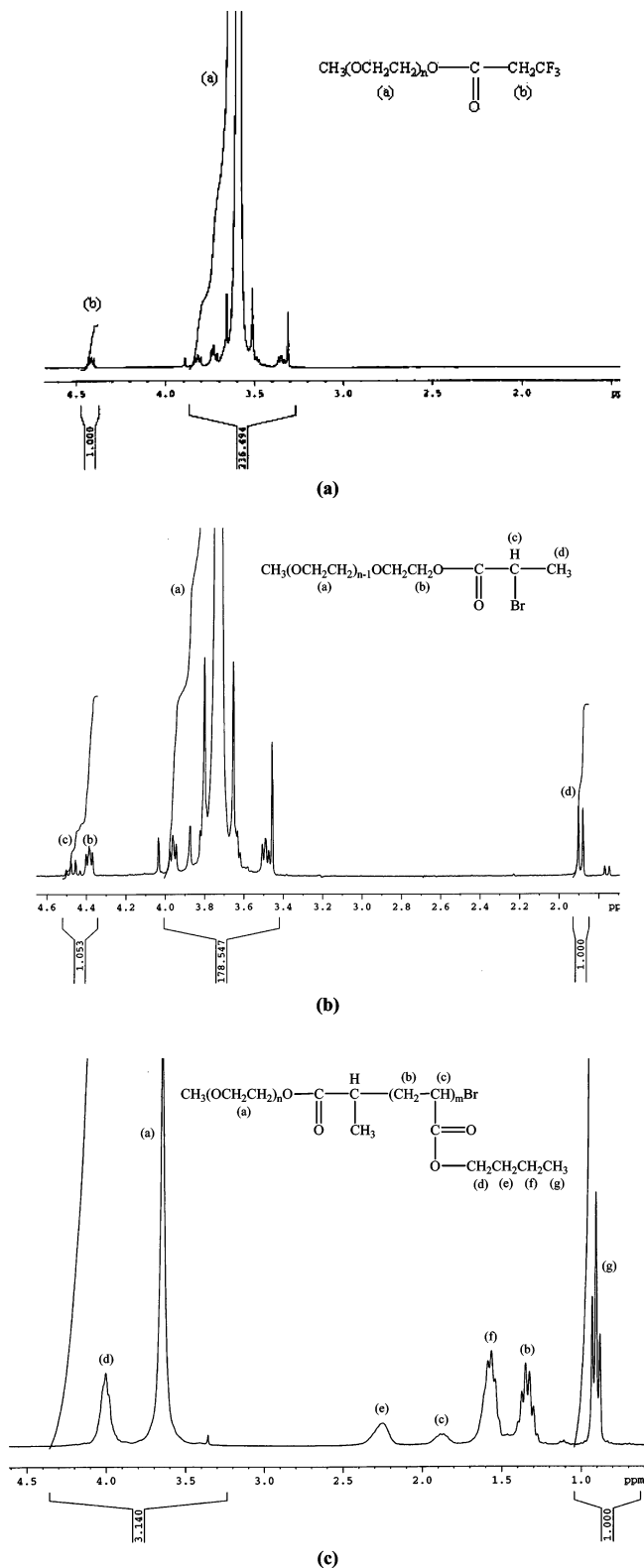


Figure 1. ¹H NMR spectra of (a) poly(ethylene oxide) monomethyl ether (PEO-ME, $M_n = 5000$ g/mol, $M_w/M_n = 1.07$) (here the hydroxyl end of the polymer was pretreated with trifluoroacetic anhydride for precise determination of OH content,³⁹ and the resonance at $\delta = 4.5$ ppm (corresponding to the terminal group $-\text{CH}_2-\text{O}-\text{CO}-\text{CF}_3$) confirms the formation of the trifluoroacetate derivative of the polymer), (b) bromopropionyl end-functionalized PEO macroinitiator derived from the PEO-ME, and (c) poly(ethylene oxide)-*b*-poly(*n*-butyl acrylate) (PEO-PnBA) synthesized using the macroinitiator ($M_n = 12\,800$ g/mol, $M_w/M_n = 1.39$).

copolymer structure is also validated by the monomodality of the molecular weight distribution obtained using GPC (Figure 2).

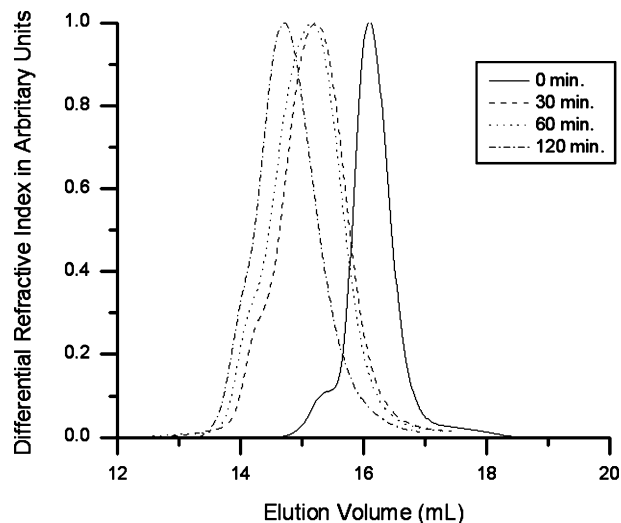


Figure 2. Gel permeation chromatography (GPC) traces demonstrating the time evolution of the molecular weight distribution of poly(ethylene oxide)-poly(*n*-butyl acrylate) in the atom transfer radical polymerization (ATRP) of *n*-butyl acrylate (nBA) at $[\text{nBA}]_0:[\text{I}]_0 = 140$ and $[\text{PMDETA}]_0:[\text{Cu(I)Br}]_0 = 4:1$.

Monomer conversion was determined from the ratio of the areas under the peaks between the “a + d” and “g” protons (Figure 1c).

2.3. Electron DFT Calculations. To estimate the enthalpy and free energy changes of reactions (ΔH and ΔG , respectively) involving PMDETA species, the C–H bond dissociation energies of all relevant substances were evaluated as follows. First, the optimal geometries of the participating molecules were determined by solving the Kohn–Sham equation¹³ for the ground-state molecular orbital wave functions.¹⁴ Computations were performed using the Gaussian03 software package within the assumption that the molecular orbital wave function is a linear combination of a finite number of the Gaussian functions in the 6-31g(d) basis set.¹⁵ In self-consistently solving the Kohn–Sham equation, the B3LYP functional was utilized to model the functional dependence of the exchange correlation energy of the Hamiltonian on the electron density. An initial guess for the molecular geometry was generated using the GaussView software for input to the subsequent geometry optimization. For each iteration of the optimization, the new geometry was computed using the Bery algorithm,¹⁶ and the iterative process was repeated until a set of convergence criteria was satisfied. Subsequently, a vibration frequency analysis was performed on the optimized geometries so obtained to include the molecular mechanical contributions associated with translational, rotational, and vibrational motions of the molecules in their ground-state enthalpy and free energy, using the Gaussian03 software. All enthalpy and free energy estimates were made at 90 °C and 1 atm on the basis of the assumption of the ideal gas behavior of the molecules and the ground-state dominance approximation. The validity of this combination of procedures and assumptions has been previously established in various ways; for instance, the same procedures predicted the heat of dissociation of methane into methyl and hydrogen radicals at 298.15 K within 0.23% of the experimental value and the heat of dissociation of propane into isopropyl and hydrogen radicals at 298.15 K within 1.25% of the experimental value.¹⁷

For calculations of the bond dissociation enthalpy and free energy of the C–H bond of the polymer species, the polymer chain-end structure was approximated by the dimer of nBA; using the nBA trimeric structure produces only a negligible difference from the dimer in the resulting estimates of the bond dissociation enthalpies and free energies, which confirms the adequacy of the dimer approximation.

2.4. Kinetic Data Modeling. For testing the proposed ATRP models, the kinetic balance equations describing the evolution of the first three moments (i.e., the zeroth, first, and second moments) of the molecular weight distributions of all species participating in

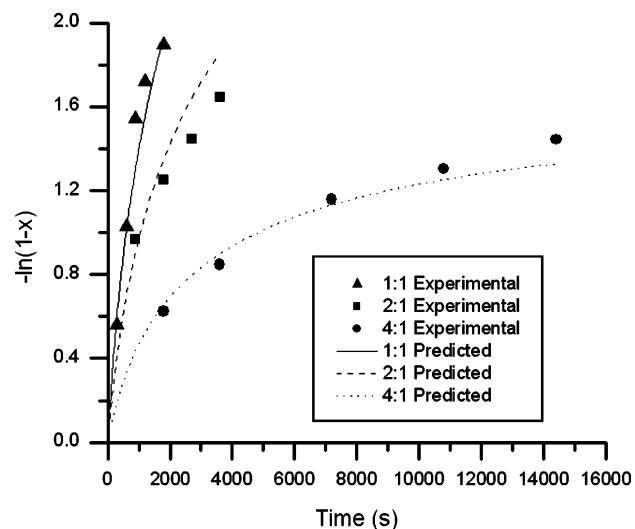


Figure 3. Evolution of $-\ln(1-x)$ in the atom transfer radical polymerization (ATRP) of *n*-butyl acrylate (nBA) at the three different ratios of $[\text{PMDETA}]_0:[\text{Cu}(\text{I})\text{Br}]_0$ (i.e., 1:1, 2:1, and 4:1); here x denotes the monomer conversion defined as $x = 1 - [\text{nBA}]/[\text{nBA}]_0$. The curves were constructed on the basis of the best-fit parameters that resulted from the least-squares fitting of the experimental conversion data using the ATRP mechanism, which accounts for all feasible reactions involving the PMDETA species but not for the difference in the reactivity between the pristine and copper-bound PMDETA molecules.

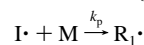
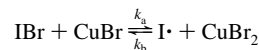
the ATRP reactions were derived, as summarized in sections 1–3 of the Supporting Information. These coupled ordinary differential equations were numerically integrated using the Adam-Gear method¹⁸ to make estimates of the molecular properties of the polymerization system including the monomer conversion ($x \equiv 1 - [\text{nBA}]/[\text{nBA}]_0$), polydispersity index (PDI, defined as the ratio \bar{M}_w/\bar{M}_n), and the fraction of dead chains produced by the chain transfer and termination reactions (f). Comparison of the model predictions of the properties to the experimental data was conducted by application of the least-squares analysis method in which the best-fit parameter condition for a given model is determined through the minimization of the objective function χ^2 , defined as $\chi^2(\mathbf{k}) = \sum_{i=1}^N (x_{\text{exp}}(t_i) - x_{\text{calc}}(t_i, \mathbf{k}))^2$, in which \mathbf{k} denotes a vector composed of all adjustable parameters of the kinetic model, $x_{\text{exp}}(t_i)$ represents the molecular property data experimentally measured at N data points (i.e., t_i , $i = 1, \dots, N$), and $x_{\text{calc}}(t_i, \mathbf{k})$ represents the properties calculated from the model for a given set of \mathbf{k} parameters at the corresponding data points. A MATLAB code on the basis of the Levenberg–Marquardt optimization method combined with the computing routine for the numerical integration of the kinetic equations was written and used to perform the nonlinear least-squares fitting of the experimental data to the proposed kinetic model. For obtaining the best-fit results, a parameter space spanning 5 orders of magnitude was searched for each variable.

3. Results and Discussion

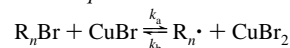
To determine how the PMDETA ligand influences the ATRP of nBA, polymerization kinetic measurements were conducted at three different ligand-to-copper initial molar concentration ratios; hereafter, this ratio will be denoted as $[\text{PMDETA}]_0:[\text{Cu}(\text{I})\text{Br}]_0$, and the values of $[\text{PMDETA}]_0:[\text{Cu}(\text{I})\text{Br}]_0$ in these experiments were 1:1, 2:1, and 4:1. For each $[\text{PMDETA}]_0:[\text{Cu}(\text{I})\text{Br}]_0$ ratio, the monomer conversion was recorded as a function of time. All measurements were performed at 90 ± 2 °C. At all conditions, catalyst solubility was maintained throughout the reaction with no discernible precipitation of the copper catalyst, and the resultant kinetic data were reproducible typically within a few percent. As displayed in Figure 3, the resulting conversion vs time data obtained at the three different ligand-to-copper ratios present a clear trend in the effect of

Table 1. Conventional Mechanism for Atom Transfer Radical Polymerization (ATRP)^a

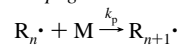
Initiation



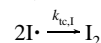
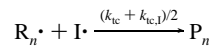
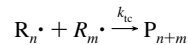
ATRP Equilibrium



Propagation



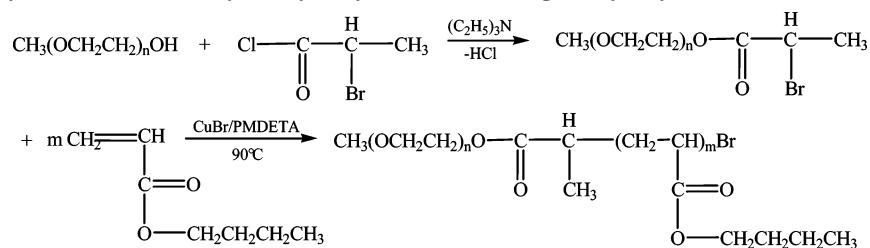
Chain Termination by Combination^b



^a See recent review by Matyjaszewski and co-workers for further information regarding the ATRP techniques and chemistries.^{1,2} Here, IBr, I[•], M, R_n[•], and P_n denote the initiator, initiator radical, monomer, living polymer radical of length n , and dead polymer chain of length n , respectively. ^b Alkyl acrylate polymerization terminates predominantly by the combination mechanism.³⁸ $k_{tc,i}$ represents the termination rate constant for the macroinitiator.

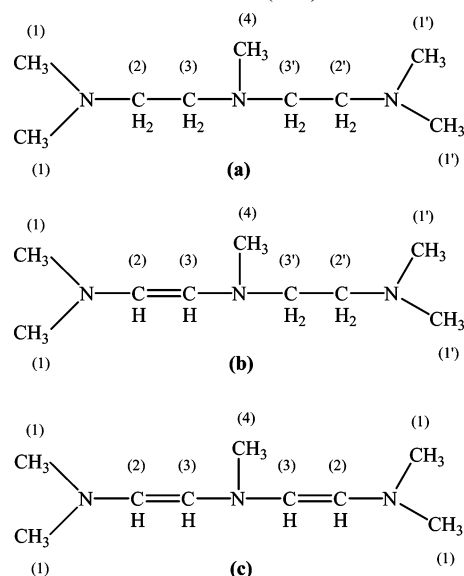
PMDETA concentration that the rate of polymerization decreases with increasing $[\text{PMDETA}]_0:[\text{Cu}(\text{I})\text{Br}]_0$, confirming previous findings from other research groups.^{11,12} These results unambiguously signify that PMDETA impedes the ATRP of nBA. One may argue that the observed qualitative trend by itself does not automatically establish whether the kinetic retardation caused by PMDETA occurs as a result of any side reaction involving radical transfer to PMDETA because any indirect influence of PMDETA on the ATRP reaction mechanisms (for instance, a shift of the activation–deactivation equilibrium toward a lower activated radical concentration induced by excess PMDETA) might also lead to a similar slowdown in the polymerization kinetics, in which case the effect of PMDETA would simply be alterations to rate constant values for the conventional ATRP component reactions of initiation, equilibrium, propagation, and termination; see Table 1 for a summary of the conventional ATRP reactions and for the definition of notations for various chemical species and rate constants. Evidence has been reported, however, that changing the ligand-to-copper ratio in the range $[\text{PMDETA}]_0:[\text{Cu}(\text{I})\text{Br}]_0 > 1:1$ has no influence on the activation rate constant (k_a).¹⁹ Although little is known in the literature, we will assume that all other rate constants (such as k_d , k_p , and k_{tc0} as defined in Table 1) are also largely insensitive to the variation of $[\text{PMDETA}]_0:[\text{Cu}(\text{I})\text{Br}]_0$ on the basis of the fact that the concentration of PMDETA in the reaction system is typically very low, i.e., less than a few wt %.

To probe whether the observed kinetic behavior in the ATRP of nBA is describable with the conventional ATRP mechanism, we performed nonlinear regression fit of the conventional ATRP model to the experimental kinetic data; based on the basic ATRP mechanism described in Table 1, the kinetic balance equations for the first three moments (i.e., the zeroth moment for the conversion data fitting, plus the first and second moments for calculating polydispersity indices (PDI) as will be discussed later in this paper) of the molecular weight distributions²⁰ of all the species participating in the polymerization reaction were established (see section 1 in the Supporting Information), and the resulting differential equations were numerically solved for the time-dependent monomer concentration, $[\text{nBA}]$, for com-

Scheme 1. Synthesis Route for Poly(*n*-butyl acrylate) (PnBA) Using a Poly(ethylene oxide) Macroinitiator

parison with the experimental conversion data. We used one set of activation, deactivation, and termination rate constants for both propionate-end-functionalized macroinitiator and propagating PnBA, since the active chain-end structures are comparable between those two species.²¹ The initiation rate constant was set equal to the propagation rate constant for nBA; this equal reactivity assumption is well justified by the long-chain nature of the initiator²² in addition to the fact that the initiator chain-end structure closely resembles that of the monomer. The remaining four kinetic constants (i.e., k_a , k_d , k_p , and k_{tc0} , as introduced in Table 1) were optimized to fit the monomer conversion profiles obtained from ATRP conducted at the three [PMDETA]₀: [Cu(I)Br]₀ ratios; to take into account a possible slowdown in the rate of combinative chain termination at high monomer conversions (due to the large sizes of living chains), we used a relation of the form $k_{tc} = k_{tc0} \text{DP}^{-(0.065+0.016\text{DP})}$ (in which k_{tc0} and DP represent the termination rate constant in the non-diffusion-controlled limit and the degree of polymerization, respectively) for estimating the k_{tc} values,²³ and an arithmetic mean was used for deducing the rate constant for the cross-termination reaction between a living chain (R_n^*) and an initiator radical (I^\bullet) from k_{tc} and $k_{tc,I}$, considering the possible effect of diffusional control of this reaction.^{20,24} We explored fairly wide ranges of parameter values for the fitting, that is, $k_a = 10^{-2}$ – $10^2 \text{ L mol}^{-1} \text{ s}^{-1}$, $k_d = 10^6$ – $10^{10} \text{ L mol}^{-1} \text{ s}^{-1}$, $k_p = 10^2$ – $10^6 \text{ L mol}^{-1} \text{ s}^{-1}$, and $k_{tc0} = 10^6$ – $10^{10} \text{ L mol}^{-1} \text{ s}^{-1}$. Because the conventional mechanism of ATRP does not include any avenue for the influence of PMDETA on the polymerization kinetics, one set of rate constants cannot capture the observed variation in the kinetics among the three different ligand concentrations. As argued above, however, PMDETA may have a subtle indirect effect on the rate constants; in this case, one should be able to model the observed difference in kinetics by utilizing rate constant values slightly differing for different ligand concentrations. We performed the four-parameter fitting of the kinetic data in which each set of conversion data were modeled independently (results not shown), and the resulting least-squares fit parameters significantly varied among the ligand-to-copper ratios; $k_a = 1.07 \times 10^{-3}$ – $1.59 \times 10^{-3} \text{ L mol}^{-1} \text{ s}^{-1}$, $k_d = 3.70 \times 10^5$ – $3.08 \times 10^6 \text{ L mol}^{-1} \text{ s}^{-1}$, $k_p = 1.75 \times 10^3$ – $1.17 \times 10^4 \text{ L mol}^{-1} \text{ s}^{-1}$, and $k_{tc0} = 1.93 \times 10^6$ – $8.49 \times 10^9 \text{ L mol}^{-1} \text{ s}^{-1}$. It is unphysical to expect variations of orders of magnitude in rate constants to arise as a result of a few wt % changes of PMDETA concentration, and we conclude that the influence of PMDETA likely entails reactions that are not considered in the conventional ATRP mechanism.

The most reasonable mechanism for the inhibition caused by PMDETA therefore appears to be a side reaction involving a radical transfer from the propagating chain to the ligand species, as has been proposed by Kubisa and co-workers.^{9,11} To test this hypothesis by modeling of the kinetic data, we developed a comprehensive ATRP model that includes the ligand transfer and other reactions that may ensue from the ligand transfer. The ligand transfer may introduce many new chemical substances in the reaction mixture and consequently many additional

Scheme 2. Nomenclature of Sites for Radical Formation on (a) *N,N,N',N',N''*-Pentamethyldiethylenetriamine (PMDETA) (L), (b) Mono-unsaturated PMDETA (L[•]), and (c) Di-unsaturated PMDETA (L^{••})

reaction steps in the polymerization mechanism, and it is impractical to incorporate all such possible reactions in the ATRP model. To identify the most plausible reaction scenarios, we analyzed the kinetic and/or thermodynamic feasibility of all possible reactions involving the species generated by the radical transfer to PMDETA. These analyses computed the enthalpies and free energies of all the reactants and products involved by solving the Kohn–Sham equations for the related molecular species using the established ab initio DFT calculation methodology; see section 2.2 for further details.

As a first step, the electron DFT calculations were performed on various ligand radical homologues to identify the most likely location of the unpaired electron generation on the PMDETA molecule. As depicted in Scheme 2a, PMDETA has four distinct protons, labeled with (1 or 1'), (2 or 2'), (3 or 3'), and (4), and depending on which of these protons is transferred to the polymer radical during the chain transfer, four different PMDETA radicals can be generated. For a family of reactions in which a living polymer chain (R_n^*) undergoes chain transfer with PMDETA (L) to generate a dead polymer chain ($R_n\text{H}$) and a PMDETA radical (L^\bullet), the enthalpies of reaction (ΔH°) were evaluated, and the results are listed in the first row of Table 2 (reaction 1). Among the four possible sites for radical formation, the PMDETA radical having an unpaired electron in position 3 in Scheme 2a has the lowest ΔH . On the basis of an assumption of the Evans–Polanyi linear relationship between activation energy (E_a) and heat of the reaction (ΔH) (i.e., $E_a = a\Delta H + b$ where a (≈ 0.65 for C–H bond dissociation reactions²⁵) and b are numerical constants),^{26–29} formation of this methylene radical, which will be referred to as $L^\bullet[3]$ hereafter (as defined in Table 2), should be the most feasible mechanism

Table 2. Summary of the Results of the Electron Density Functional Theory (DFT) Calculations^a

reaction ID (type)	reactants ^b	possible products ^b	ΔH (kcal/mol)	ΔG (kcal/mol)	
1 (transfer)	L + R_n·	L·[1]	R_nH	7.04	7.18
		L·[2]		4.85	6.19
		L·[3]		2.46	4.03
		L·[4]		4.38	4.82
2 (transfer)	L·[3] + R _n ·	·L·[3,1]	R _n H	6.80	7.82
		·L·[3,1']		5.21	6.15
		·L·[3,2]		1.39	2.53
		·L·[3,2']		4.35	4.76
		·L·[3,3']		9.73	12.04
		·L·[3,4]		12.46	12.91
3 (termination)	L·[3] + R_n·	L ^{=c}	R _n H	-47.47	-44.55
		L	P_n⁼	-59.72	-57.81
4 (termination)	L·[3] + L·[3]	L-L	-	-49.95	-29.21
		L⁼	L	-49.94	-48.58
5 (transfer)	L⁼ + R_n·	L ⁼ ·[1]	R_nH	3.87	4.25
		L ⁼ ·[1']		6.32	6.26
		L ⁼ ·[2]		16.79	16.62
		L ⁼ ·[2']		4.20	5.28
		L ⁼ ·[3]		12.75	11.83
		L⁼·[3]		1.51	1.89
		L ⁼ ·[4]		2.97	3.18
		·L ⁼ ·[3',1]	R _n H	7.20	8.80
6 (termination)	L ⁼ ·[3'] + R _n ·	·L ⁼ ·[3',1']		6.63	8.25
		·L ⁼ ·[3',2]		15.05	15.23
		·L ⁼ ·[3',2']		1.69	2.92
		·L ⁼ ·[3',3]		18.89	19.71
		·L ⁼ ·[3',4]		10.47	12.26
		L ⁼ ·[3'] + R _n ·	R _n H	-46.23	-43.38
7 (termination)	L⁼·[3'] + R_n·	L ⁼	P_n⁼	-58.76	-55.66
		L ⁼ -L ⁼	-	-47.00	-26.53
8 (termination)	L⁼·[3'] + L⁼·[3']	L ⁼ ₌	L⁼	-47.74	-45.27
		L ⁼ -L	-	-51.40	-30.16
9 (termination)	L⁼·[3'] + L·[3]	L ⁼ ₌	L	-48.70	-47.42
		L ⁼	L⁼	-48.98	-46.44
		L ⁼ ·[1]		4.81	5.59
10 (transfer)	L⁼₌ + R_n·	L ⁼ ·[2]	R_nH	14.63	14.54
		L ⁼ ·[3]		14.11	14.82
		L ⁼ ·[4]		4.37	5.75
		Cu-L·[1]	R_nH	dnc ^e	dnc ^e
11 (transfer)	Cu-L + R_n·	Cu-L·[2]		dnc ^e	dnc ^e
		Cu-L·[3]		4.65	5.27
		Cu-L·[4]		6.00	7.12

^a Shown in bold typeface are the reactions which are incorporated into the proposed mechanism for the *N,N,N',N',N''*-pentamethyldiethylenetriamine (PMDETA)-based atom transfer radical polymerization (ATRP) of *n*-butyl acrylate (nBA) based on the analyses of the enthalpy and free energy changes of reaction (ΔH and ΔG , respectively); see the text in section 3 for a detailed discussion. ^b Numbers enclosed in the square brackets indicate the positions of unpaired electrons on the ligand with reference to the nomenclature defined in Scheme 2. ^c Mono-unsaturated PMDETA species produced from L·[3]. The chemical structure of L⁼ is given in Scheme 2b. ^d Di-unsaturated PMDETA species produced from L⁼·[3']. The chemical structure of L⁼₌ is shown in Scheme 2c. ^e Calculations failed to converge to an optimal geometry.

of the ligand transfer in terms of its reaction rate. By applying the Arrhenius relation between reaction rate constant and activation energy (i.e., $k \sim \exp(-E_a/RT)$ where E_a linearly scales with ΔH), the difference of about 2 kcal/mol between the ΔH values for formation of L·[3] can be translated into nearly an order-of-magnitude difference in the estimates of the reaction rates and implies that the relative frequency of generation of other radicals is negligible to a reasonable approximation. Thus, for all practical purposes to model the polymerization kinetic data, we consider L·[3] as the sole PMDETA radical generated by chain transfer. On the basis of a previous electron spin resonance (ESR) spectroscopy study of the radical formation from a similar ligand molecule, *N,N,N',N'*-tetramethylethylenediamine (TMEDA),³⁰ the methylene radical of L·[3] (or even L·[2]) should not be able to reinitiate polymerization of nBA, whereas L·[1] and L·[4] (i.e., those created upon removal of a proton from the methyl group) are likely to react with the nBA monomers. Thus, our hypothesis for the ligand transfer mechanism is consistent with the reported results of the MALDI-TOF mass spectroscopy analysis of ATRP-synthesized PnBA samples, which confirm the absence of polymer chains containing initiating-ligand fragments.^{9,11}

Once generated, L·[3] may react with another living polymer chain (R_n·) to undergo chain transfer and lose one more proton to become a diradical (·L·). In this case, as summarized in the second row of Table 2 (reaction 2), L·[3] may lose a proton from six different sites (i.e., positions 1, 2, 4, 1', 2', and 3', as defined in Scheme 2a), resulting in six distinct PMDETA diradicals (i.e., ·L·[3,1], ·L·[3,2], ·L·[3,4], ·L·[3,1'], ·L·[3,2'], and ·L·[3,3']) using the notation introduced in the table). The ΔH values estimated for the respective reactions suggest that it is most likely that L·[3] will lose its proton from position 2, thereby forming the ·L·[3,2] diradical species. Again, on the basis of the Arrhenian assumption (i.e., $k \sim \exp(-\Delta H/RT)$), the relative probability for the formation of other diradicals should be kinetically ignorable compared to the ·L·[3,2] diradical, which allows us to exclude the diradical formation reactions in the ATRP mechanism other than the one resulting in ·L·[3,2]. We believe that ·L·[3,2] will further stabilize itself by sharing the two unpaired electrons on the carbon atoms labeled as (3) and (2) in Scheme 2a to form a double bond between the carbons; this reaction involves huge negative values of $\Delta H = -48.87$ kcal/mol and $\Delta G = -47.08$ kcal/mol, as estimated from the data listed for reactions 2 and 3 in Table 2,

and these estimates are consistent with the known value of $\Delta H = +68$ kcal/mol for the bond dissociation energy of the π bond of ethylene's carbon-carbon double bond.³¹ Thus, the additional chain transfer to $L\cdot[3]$ will eventually lead to generation of a dead polymer chain (R_nH) and a mono-unsaturated ligand (L^\ominus); the exact chemical structure of L^\ominus is shown in Scheme 2b.

There are two other possible routes by which a reaction between $L\cdot[3]$ and $R_n\cdot$ can lead to radical termination. First, $L\cdot[3]$ and $R_n\cdot$ may combine to form an R_nL molecule, which is unlikely considering the previous MALDI-TOF data of Kubisa and co-workers in which no evidence of R_nL has been detected from the PMDETA-based ATRP of nBA.¹¹ A second possibility is that $L\cdot[3]$ and $R_n\cdot$ exchange an electron by disproportionation, regenerating an original ligand (L) plus a unsaturated dead polymer (P_n^\ominus). In fact, this disproportionation reaction appears to involve a more negative ΔH (and a more negative ΔG as well) than the L^\ominus formation reaction (discussed in the previous paragraph), as listed in Table 2 (reaction 3). On the basis of these heat of reaction estimates, only the mechanism of disproportionation was included in the modeling of reactions involving $L\cdot[3]$ and $R_n\cdot$.

Regarding possible reactions of $L\cdot[3]$, now what remains unexplored is whether and how the $L\cdot[3]$ ligand radical reacts with another $L\cdot[3]$ molecule in the reaction mixture. Just like in the case of reactions between $L\cdot[3]$ and $R_n\cdot$, annihilation of two $L\cdot[3]$ radicals may occur by two routes, that is, combination and/or disproportionation. In determining the dominance of one mechanism over the other, it should be realized that these two reactions yield very disparate reaction products (as can be seen in the fourth row of Table 2), which makes the Evans-Polanyi correlation nonapplicable because of the likelihood of the difference in the transition state of the termination reaction between the combination and disproportionation mechanisms, as can be inferred from the original discussion of Evans and Polanyi.²⁹ Therefore, we relied on a comparison of the ΔG values to select a more realistic termination path. As shown in the fourth row of Table 2, the disproportionation reaction, which converts two $L\cdot[3]$ radicals to L^\ominus and L , offers a thermodynamically far more favorable pathway for termination than the combination mechanism; the combination leaves a compound ligand molecule (denoted as $L-L$ in Table 2) which is expected to suffer severe steric repulsion between the two precursor structures, as reflected in the correspondingly higher ΔG value.

The L^\ominus mono-unsaturated ligand (Scheme 2b) may undergo radical transfer reactions involving the transfer of a proton from L^\ominus in positions 1, 1', 2, 2', 3, 3', and 4 (defined in Scheme 2b) to $R_n\cdot$, yielding seven different mono-unsaturated ligand radicals, denoted as $L^\ominus\cdot[1]$, $L^\ominus\cdot[1']$, $L^\ominus\cdot[2]$, $L^\ominus\cdot[2']$, $L^\ominus\cdot[3]$, $L^\ominus\cdot[3']$, and $L^\ominus\cdot[4]$ in Table 2. The ΔH values for the corresponding transfer reactions are listed in the fifth row of Table 2. Clearly the kinetically most feasible site for radical formation on L^\ominus is the 3' position.

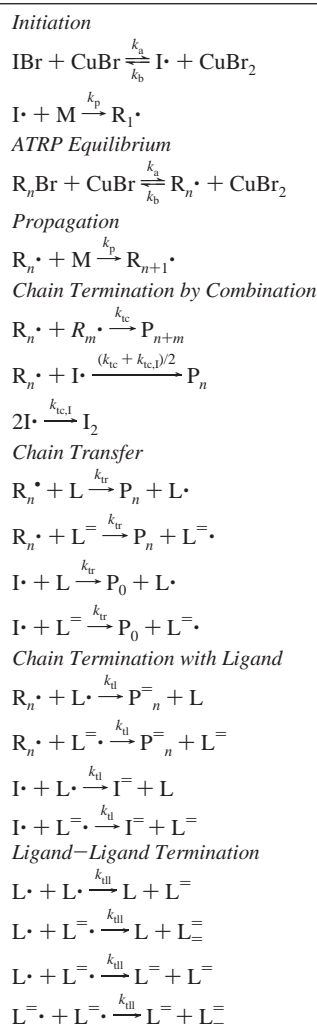
This mono-unsaturated ligand radical, which will be designated as $L^\ominus\cdot[3']$ hereafter, may react with $R_n\cdot$ or with a monomer molecule in a number of ways, just like $L\cdot[3]$ may do so. Again, the possibilities of reinitiation upon reaction of $L^\ominus\cdot[3']$ with a monomer and combination between $L^\ominus\cdot[3']$ and $R_n\cdot$ were not considered on the basis of the work of Kubisa and co-workers.¹¹ As for possible radical transfer reactions with $R_n\cdot$ to form mono-unsaturated diradicals (i.e., a family of species which are referred to as $\cdot L^\ominus\cdot$ in Table 2), the kinetically most favored site for the abstraction of a proton from $L^\ominus\cdot[3']$ is position 2', as supported by the ΔH estimates for all possible mono-unsaturated diradicals

(i.e., $\cdot L^\ominus\cdot[3',1]$, $\cdot L^\ominus\cdot[3',1']$, $\cdot L^\ominus\cdot[3',2]$, $\cdot L^\ominus\cdot[3',2']$, $\cdot L^\ominus\cdot[3',3]$, and $\cdot L^\ominus\cdot[3',4]$) listed in the sixth row of Table 2. The resulting mono-unsaturated diradical, $\cdot L^\ominus\cdot[3',2']$, is expected to spontaneously convert to a corresponding di-unsaturated ligand denoted as $L^\ominus=$ in Table 2 (see Scheme 2c for the chemical structure of $L^\ominus=$), because of the large negative values of $\Delta H = -47.93$ kcal/mol and $\Delta G = -46.31$ kcal/mol for the transformation of $\cdot L^\ominus\cdot[3',2']$ to $L^\ominus=$, as can be calculated using the ΔH and ΔG values for reactions 6 and 7 in Table 2; therefore, the net result of the radical transfer from a living chain ($R_n\cdot$) to a mono-unsaturated ligand radical ($L^\ominus\cdot[3']$) is a generation of a dead chain (R_nH) and a new di-unsaturated ligand ($L^\ominus=$). However, as was the case with $L\cdot[3]$, we found that it is thermodynamically more feasible that a reaction between $R_n\cdot$ and $L^\ominus\cdot[3']$ yields a dead chain bearing a unsaturated end (P_n^\ominus) and a mono-unsaturated ligand (L^\ominus) through disproportionation; see the seventh row of Table 2 for a comparison of the ΔH and ΔG values between the chain transfer vs disproportionation mechanisms.

Termination of the $L^\ominus\cdot[3']$ radical can occur by bimolecular reaction between two identical $L^\ominus\cdot[3']$ radicals. A comparison of the ΔG values for the corresponding combination and disproportionation reactions (reactions 8 in Table 2) suggests that disproportionation is thermodynamically preferred in this case, resulting in $L^\ominus=$ and L^\ominus . It is also possible that $L^\ominus\cdot[3']$ undergoes termination with the saturated $L\cdot[3]$ radical, and from DFT ΔG calculations, a disproportionation that reproduces two mono-unsaturated ligand molecules (L^\ominus) was estimated to be the most plausible mechanism for this cross-termination reaction involving $L^\ominus\cdot[3']$ and $L\cdot[3]$, as can be seen from the data shown in reaction 9 of Table 2.

A radical transfer reaction may also take place between a living chain ($R_n\cdot$) and a double-unsaturated ligand molecule ($L^\ominus=$). In consequence of such reactions, four different di-unsaturated ligand radicals can be created; these radicals can be written as $L^\ominus= \cdot[1]$, $L^\ominus= \cdot[2]$, $L^\ominus= \cdot[3]$, and $L^\ominus= \cdot[4]$ using the nomenclature for the radical numbers defined in Scheme 2c. As shown in the tenth row of Table 2, $L^\ominus= \cdot[4]$ seems to be kinetically most favorable of all possible radicals that can be derived from $L^\ominus=$. However, ΔH and ΔG of the reaction yielding $L^\ominus= \cdot[4]$ are significantly larger in comparison to other chain transfer reactions (i.e., the ones that generate the $L\cdot[3]$ and $L^\ominus\cdot[3']$ radicals). Therefore, we preclude the incorporation of reactions of $L^\ominus=$ with $R_n\cdot$ in the ATRP model, and the possibility that any new species might be generated thereupon is curtailed at this stage.

On the basis of the reaction feasibility analyses as documented in Table 2, we incorporate all the suspected reactions that are considered to be highly possible into the ATRP mechanism; as summarized in Table 3, the revised ATRP model now includes 12 additional reaction steps originating from the radical transfer to ligand, as shown under the subcategories of Chain Transfer, Chain Termination with Ligand, and Ligand-Ligand Termination in Table 3. On the basis of this proposed ATRP model, a set of kinetic balance equations for all the small molecule species involved and also for the first three moments of the chain length distributions were formulated: see section 2 in the Supporting Information for details. By numerical integration of these differential balance equations, the time evolutions of the concentrations of all species and the individual moments were calculated as functions of the six rate constants, k_a , k_d , k_p , k_{tr} , k_{tl} , and k_{tll} defined in Table 3, to model simultaneously all three sets of the experimental conversion data obtained at the ligand-to-copper ratios of $[PMDETA]_0:[Cu(I)Br]_0 = 1:1, 2:1, \text{ and } 4:1$.

Table 3. Proposed Mechanism for the ATRP of nBA Using the Cu(I)Br/PMDETA Catalyst System**Table 4. Optimal Parameters Obtained from the Fitting of the Proposed ATRP Model to the Experimental Conversion Data**

parameter (units)	optimal value (range for parameter search)
k_a (L mol ⁻¹ s ⁻¹)	0.34 (10 ⁻² –10 ²)
k_d (L mol ⁻¹ s ⁻¹)	3.10×10^7 (10 ⁶ –10 ¹⁰)
k_{tr} (L mol ⁻¹ s ⁻¹)	2.40×10^3 (10 ² –10 ⁶)
k_{tl} (L mol ⁻¹ s ⁻¹)	1.93×10^{-2} (10 ⁻⁴ –10 ⁰)
k_{ll} (L mol ⁻¹ s ⁻¹)	2.70×10^{-3} (10 ⁻⁵ –10 ⁻¹)
α (dimensionless)	2.58 (10 ⁻² –10 ²)

For the rate constant for termination by combination, we used the value of $k_{tc0} = 1 \times 10^8$ L mol⁻¹ s⁻¹ taken from the literature,²¹ and as regards the adjustable fitting variables, extensive ranges (refer to Table 4) were explored in fitting the combined ATRP model to the kinetic data. As shown in Figure 3, the resulting least-squares fit is unable to reproduce the quantitative features of the experimental data with the errors associated with the kinetic measurements. The best fit parameters (for instance, $k_a = 1.01 \times 10^{-2}$ L mol⁻¹ s⁻¹ and $k_p = 2.01 \times 10^6$ L mol⁻¹ s⁻¹) significantly deviate from the known literature values,^{19,32} which is physically untenable. Furthermore, the converged fitting results yield predictions for the values of the polydispersity indices for the polymer chains in the range of 1.3–2.8, which is far above the experimental values of 1.1–1.4 (as discussed later in the paper). All these inconsistencies suggest that the proposed ATRP model is still defective in some respect.

An important clue for further improving the ATRP model comes from a previous extended X-ray absorption fine structure (EXAFS) study^{33,34} of complexes formed between PMDETA and copper for both Cu(I)Br and Cu(II)Br₂, which indicates that the structure of the complex typically contains one PMDETA molecule and one copper atom per complex.^{12,13} Thus, in a polymerization with an excess of ligand (i.e., [PMDETA]₀: [Cu(I)Br]₀ > 1:1), two distinct ligand species may exist in the system: one bound to the copper and the other in the free unbound state. These two types of ligands are expected to differ from each other in their chemical reactivity, on account of the different chemical environment that would be brought about by the binding of the ligand to the copper atom. The complexation of the PMDETA ligand with Cu(I) or Cu(II) involves donation of the lone pairs of electrons from the nitrogen atoms of PMDETA to empty 3d orbitals of Cu(I) or Cu(II), resulting in a deficiency of electron density in PMDETA.³⁵ The electron-deficient PMDETA molecule should be less willing to form a radical, and consequently the tendency of copper-bound ligand to undergo chain transfer is expected to be lower. This reasoning regarding the reactivity of the copper-bound PMDETA is further supported by calculations of ΔH and ΔG for the radical transfer from a living chain (R_n[·]) to a copper-bound PMDETA molecule (Cu–L), leading to a formation of the PMDETA radical bound to the copper with a unpaired electron in position 3 of the PMDETA structure (Scheme 2a); hence, the resulting radical is denoted Cu–L·[3]. As shown in the 11th row of Table 2, indeed the free unbound ligand is estimated to be thermodynamically more prone to the radical formation than its copper-bound analogue. To account for a possible discrepancy in the reactivity between the two different states in which PMDETA can exist, we incorporated into the ATRP kinetic model an additional floating parameter α , defined as the ratio of the transfer rate constant k_{tr} of a free ligand (L) to the transfer rate constant k_{tr} of a copper-bound ligand (Cu–L). Analogously, the same factor α was introduced to account for possible differences in all other rate constants for reactions involving PMDETA and its derivatives (i.e., k_{tl} and k_{ll}) between the two ligand types; see section 3 in the Supporting Information for the details of the corresponding changes made in the ATRP model. Again with this modified ATRP model, least-squares analyses of the kinetic data were performed using k_a , k_d , k_{tr} , k_{tl} , k_{ll} , and α as the fitting variables with k_p being set at the literature value of 5.63×10^4 L mol⁻¹ s⁻¹,³² and we found that the final version of the ATRP model is capable of providing a complete description of the experimental conversion profiles simultaneously for all three ligand-to-copper ratios, as displayed in Figure 4; the resulting fits give remarkable agreement with all data points within the few percent deviations.

The optimized fit parameters and the respective ranges of parameter values for which optimization was constrained are collected in Table 4. The k_a and k_d values obtained from a least-squares fit of the kinetic data with the ATRP model (i.e., $k_a = 0.34$ L mol⁻¹ s⁻¹ and $k_d = 3.10 \times 10^7$ L mol⁻¹ s⁻¹, giving rise to an estimation for the activation–deactivation equilibrium constant of K ($\equiv k_a/k_d$) = 1.10×10^{-8} , at 90 °C) are in reasonable agreement with the values for the same rate and equilibrium constants estimated by other research groups; for example, $K \approx 10^{-8}$ for the ATRP of methyl acrylate at 90 °C using the Cu(I)Br/PMDETA combination,³⁶ and $k_a \approx 10^{-3}$ – 10^{-2} L mol⁻¹ s⁻¹ for bromine-terminated *tert*-butyl acrylate dimer in equilibrium with Cu(I)Br/bipyridine at 35 °C.¹⁹ The best-fit value for k_{tr} (2.40×10^3 L mol⁻¹ s⁻¹ at 90 °C) is consistent with that previously reported by Kubisa and co-

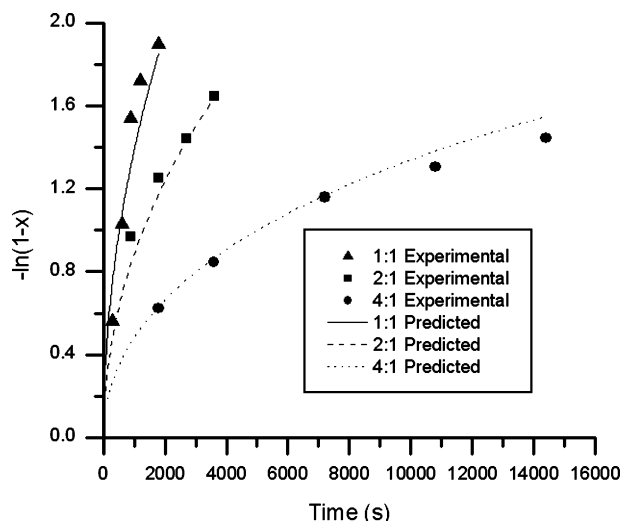


Figure 4. Evolution of $-\ln(1-x)$ in the ATRP of nBA at the three different ratios of $[\text{PMDETA}]_0:[\text{Cu(I)Br}]_0$. The curves were constructed on the basis of the best fit parameters (Table 4) that resulted from the least-squares fitting of the experimental conversion data using the proposed ATRP mechanism which accounts for all feasible reactions involving the PMDETA species and the difference in the reactivity between the pristine and copper-bound PMDETA molecules; the proposed ATRP mechanism is summarized in Table 3.

workers ($3.3 \times 10^3 \text{ L mol}^{-1} \text{ s}^{-1}$ at 25°C); the small discrepancy may have been due to the fact that they estimated the rate constant by model fitting of kinetic data obtained from heterogeneous ATRP reactions for which any kinetic model in fact loses its applicability. Important outcomes from the kinetic modeling include determination of the rate constants for the nonconventional reactions (i.e., $k_{\text{tl}} = 1.93 \times 10^{-2} \text{ L mol}^{-1} \text{ s}^{-1}$ for termination with ligand and $k_{\text{tll}} = 2.70 \times 10^{-3} \text{ L mol}^{-1} \text{ s}^{-1}$ for ligand–ligand termination) which are previously unknown. It should be noted that the resulting values are many orders of magnitude smaller than the literature value of $k_{\text{tc}} = 1 \times 10^8 \text{ L mol}^{-1} \text{ s}^{-1}$ for the chain termination reactions²¹ and are quite consistent with high chemical stability of the ligand radicals (i.e., the species referred to as $\text{L}\cdot[3]$ and $\text{L}^{\cdot}[3']$ in Table 2) previously observed by other researchers.^{11,30} The low reactivity of $\text{L}\cdot[3]$ and $\text{L}^{\cdot}[3']$ also provides a posteriori justification of the use of a single rate constant (k_{tl}) for different ligand–ligand termination reactions (Table 3) in the kinetic modeling; because of the extremely slow rates of chain termination with ligand and ligand–ligand termination, the concentrations of L^{\cdot} and thus $\text{L}^{\cdot}[3']$ are expected to stay very low over most of the conversion, making little contribution to the overall ATRP mechanism, and thus disregarding possible variations of the rates among different ligand–ligand termination reactions has negligible impact on the modeling. The same can be said about the use of one rate constant (k_{tl}) for the reactions of chain termination with ligand (Table 3). The α value of 2.58 suggests that PMDETA is more susceptible to the radical transfer in the free state than when it is bound to copper, as predicted by DFT calculations, and quantification of the difference in reactivity between the free and copper-bound ligands is a crucial ingredient in the ATRP modeling.

The uncertainties associated with the estimated rate constants (i.e., k_a , k_d , k_{tr} , and α) are small. This was confirmed by examining the parametric sensitivity of the model predictions. We present plots in section 5 of the Supporting Information which demonstrate that, for example, a factor of 2 increase or decrease of the individual parameters from their best-fit values causes significant deviations of the kinetic predictions from the

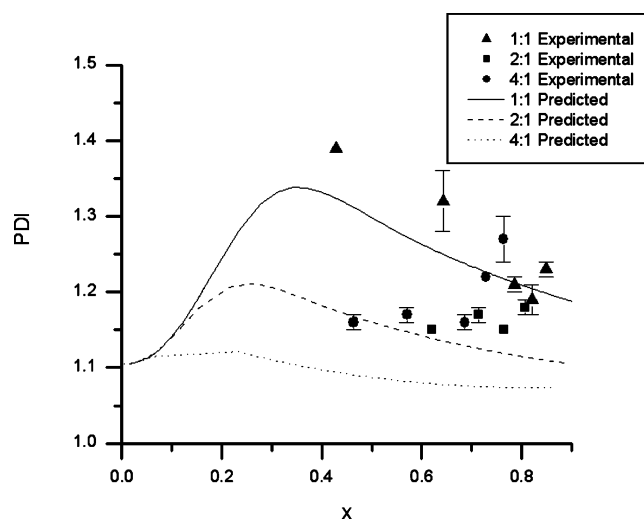


Figure 5. Comparison between the model predictions (continuous curves) and the experimental data (discrete points) for the polydispersity index (PDI). The data points with error bars represent average PDI values obtained from two separate gel permeation chromatography (GPC) measurements.

measurements, indicating that the predictions are precise to within at least this factor of the respective estimate. The same analysis, on the other hand, suggests that the precision of the estimate for k_{tll} is approximately within an order of magnitude or two (as shown in section 5 of the Supporting Information). As for the rate constant k_{tl} to which the polymerization kinetics is largely insensitive (Supporting Information) because of its relatively small value and the small concentrations of the species participating in the corresponding reactions (i.e., R_n^{\cdot} , $\text{I}\cdot$, $\text{L}\cdot$, and L^{\cdot}), it is not feasible to establish the preciseness of its estimate. The absolute uncertainty for this case is nonetheless expected to be in the range similar to that of k_{tll} because these two reactions are similar in their mechanisms.

A further test for consistency of the best-fit results listed in Table 4 with experimental PDI data was conducted. As presented in Figure 5, solely based on the parameter values determined from the fitting, the proposed ATRP model predicts time-dependent PDI traces for varying ratios of $[\text{PMDETA}]_0:[\text{Cu(I)Br}]_0$ which compare satisfactorily with the PDI values determined experimentally from gel permeation chromatography (GPC) measurements; section 4 in the Supporting Information provides additional details regarding the estimation of the (absolute) PDI values. As shown in the figure, the measurements suggest the following trends: (i) the PDI decreases as the $[\text{PMDETA}]_0:[\text{Cu(I)Br}]_0$ ratio goes from 1:1 to 2:1 to 4:1 (that is, as the chain transfer becomes more pronounced); (ii) at the ratio of $[\text{PMDETA}]_0:[\text{Cu(I)Br}]_0 = 4:1$, the PDI is initially high and continually reduces as conversion increases, while the PDI is almost constant (over conversions studied) when $[\text{PMDETA}]_0:[\text{Cu(I)Br}]_0 = 1:1$.⁴⁰ The model captures similar trends (Figure 5); the model's predictions for the evolution of number- and weight-average chain lengths, which is responsible for the observed trends in the PDI, are presented in section 6 of the Supporting Information. There exists a discrepancy between the model prediction and the experimental measurement, and the experimental PDI values are systematically higher than those calculated. This difference is understandable in that the molecular weight distribution measured by GPC is subject to broadening due to random diffusion of polymer molecules during the elution process.³⁷ Also, lack of information regarding the swelling characteristics of the diblock copolymer and the differential refractive indices of PEO and PnBA in THF at the

measurement temperature (i.e., 30 °C) makes it impractical to attempt to accurately model the data. For these reasons, we do not intend to use the GPC data as the quantitative basis for evaluating the mechanisms of the ATRP reactions in the first place. Nonetheless, the prediction is within less than 0.1 below the measured polydispersity for all conditions tested, and this level of agreement between the prediction and observation supports the validity of the proposed model and the kinetic fitting parameters.

4. Conclusion

Studies (combining ATRP kinetic measurements, electron-DFT reaction pathway analysis, and least-squares fitting of the kinetic data using a model inferred from the DFT calculations) were performed to explore the detailed chemistries of the reactions that the PMDETA species would entail in the ATRP of nBA based on the Cu(I)Br/PMDETA catalyst system. The resultant ATRP mechanism that we propose contains three important findings: (a) the chain transfer to ligand involves the abstraction of a proton from the PMDETA ligand which occurs only at a carbon atom next to the nitrogen atom in the center of the molecule (see Scheme 2 for the chemical structure of PMDETA), producing the L•[3] radical species as defined in Table 2; (b) the PMDETA radical generated from the chain transfer reaction (i.e., L•[3]) is effectively inactive; once generated, the ligand radical is unlikely to be involved in any further reaction afterward (even including termination reactions between ligand radicals or between ligand and polymer radicals); (c) there appears to exist a significant difference in the reactivity of PMDETA toward side reactions (such as the chain-transfer reaction) between the pristine and copper-bound states (that is, the ligand becomes significantly less prone to the radical formation when it is complexed with copper). The results provide a valuable mechanistic model for predicting the molecular properties of poly(alkyl acrylate) polymers prepared using the copper/PMDETA-based ATRP techniques.

Supporting Information Available: Kinetic balance equations describing the evolution of the moments of the molecular weight distributions of all species participating in the ATRP reactions (sections 1–3), procedures for the PDI calculations (section 4), demonstration of the sensitivity of the ATRP model to variations of the rate constants (section 5), and model predictions for number and weight-average chain lengths and polydispersity as functions of conversion (section 6). This material is available free of charge via the Internet at <http://pubs.acs.org>.

References and Notes

- Patten, T. E.; Matyjaszewski, K. *Adv. Mater.* **1998**, *10*, 901–915.
- Matyjaszewski, K.; Xia, J. *Chem. Rev.* **2001**, *101*, 2921–2990.
- Wang, J. S.; Matyjaszewski, K. *J. Am. Chem. Soc.* **1995**, *117*, 5614–5615.
- Kato, M.; Kamigaito, M.; Sawamoto, M.; Higashimura, T. *Macromolecules* **1995**, *28*, 1721–1723.
- Xia, J.; Matyjaszewski, K. *Macromolecules* **1997**, *30*, 7697–7700.
- Qiu, J.; Matyjaszewski, K.; Thouin, L.; Amatore, C. *Macromol. Chem. Phys.* **2000**, *201*, 1625–1631.
- Venkatesh, R.; Harrison, S.; Haddleton, D. M.; Klumperman, B. *Macromolecules* **2004**, *37*, 4406–4416.
- O'Reilly, R. K.; Gibson, V. C.; White, A. J. P.; Williams, D. J. *Polyhedron* **2004**, *23*, 2921–2928.
- Bednarek, M.; Biedron, T.; Kubisa, P. *Macromol. Rapid Commun.* **1999**, *20*, 59–65.
- Roos, S. G.; Muller, A. H. E. *Macromol. Rapid Commun.* **2000**, *21*, 864–867.
- Bednarek, M.; Biedron, T.; Kubisa, P. *Macromol. Chem. Phys.* **2000**, *201*, 58–66.
- Huang, J.; Pintauer, T.; Matyjaszewski, K. *J. Polym. Sci., Part A: Polym. Chem.* **2004**, *42*, 3285–3292.
- Kohn, W.; Sham, L. J. *Phys. Rev. A* **1965**, *140*, 1133–1138.
- Hohenberg, P.; Kohn, W. *Phys. Rev. B* **1964**, *136*, 864–871.
- Frisch, M. J.; Trucks, G. W.; Schlegel, H. B.; Scuseria, G. E.; Robb, M. A.; Cheeseman, J. R.; Montgomery, J. A., Jr.; Vreven, T.; Kudin, K. N.; Burant, J. C.; Millam, J. M.; Iyengar, S. S.; Tomasi, J.; Barone, V.; Mennucci, B.; Cossi, M.; Scalmani, G.; Rega, N.; Petersson, G. A.; Nakatsuji, H.; Hada, M.; Ehara, M.; Toyota, K.; Fukuda, R.; Hasegawa, J.; Ishida, M.; Nakajima, T.; Honda, Y.; Kitao, O.; Nakai, H.; Klene, M.; Li, X.; Knox, J. E.; Hratchian, H. P.; Cross, J. B.; Bakken, V.; Adamo, C.; Jaramillo, J.; Gomperts, R.; Stratmann, R. E.; Yazyev, O.; Austin, A. J.; Cammi, R.; Pomelli, C.; Ochterski, J. W.; Ayala, P. Y.; Morokuma, K.; Voth, G. A.; Salvador, P.; Dannenberg, J. J.; Zakrzewski, V. G.; Dapprich, S.; Daniels, A. D.; Strain, M. C.; Farkas, O.; Malick, D. K.; Rabuck, A. D.; Raghavachari, K.; Foresman, J. B.; Ortiz, J. V.; Cui, Q.; Baboul, A. G.; Clifford, S.; Cioslowski, J.; Stefanov, B. B.; Liu, G.; Liashenko, A.; Piskorz, P.; Komaromi, I.; Martin, R. L.; Fox, D. J.; Keith, T.; Al-Laham, M. A.; Peng, C. Y.; Nanayakkara, A.; Challacombe, M.; Gill, P. M. W.; Johnson, B.; Chen, W.; Wong, M. W.; Gonzalez, C.; Pople, J. A. *Gaussian, Inc.*, 2004.
- Peng, C.; Ayala, P. Y.; Schlegel, H. B.; Frisch, M. J. *J. Comput. Chem.* **1996**, *17*, 49–56.
- Johnson III, R. D. Release 12 (Aug 2005) ed.
- Gupta, S. K. *Numerical Methods for Engineers*; New Age International: New Delhi, India, 1995.
- Nanda, A. K.; Anantchenko, G.; Matyjaszewski, K. *Polym. Prepr.* **2002**, *43*, 225–226.
- Dotson, N. A.; Galvan, R.; Laurence, R. A.; Tirrell, M. *Polymerization Process Modeling*; John Wiley and Sons: New York, 1996.
- Ziegler, M. J.; Matyjaszewski, K. *Macromolecules* **2001**, *34*, 415–424.
- Walbiner, M.; Wu, J. Q.; Fischer, H. *Helv. Chim. Acta* **1995**, *78*, 910–924.
- Shipp, D. A.; Matyjaszewski, K. *Macromolecules* **1999**, *32*, 2948–2955.
- Smoluchowski, M. *Z. Phys. Chem.* **1918**, *92*, 129–168.
- Dean, A. M. *AIChE Symp. Ser.* **2001**, *97*, 84–96.
- Evans, M. G.; Polanyi, M. *Trans. Faraday Soc.* **1935**, *31*, 875–893.
- Evans, M. G.; Polanyi, M. *Trans. Faraday Soc.* **1936**, *32*, 1333–1359.
- Evans, M. G.; Polanyi, M. *Trans. Faraday Soc.* **1937**, *33*, 448–452.
- Evans, M. G.; Polanyi, M. *Trans. Faraday Soc.* **1938**, *34*, 11–23.
- Feng, X. D.; Guo, X. Q.; Qiu, K. Y. *Makromol. Chem.* **1988**, *189*, 77–83.
- Fessenden, R. J.; Fessenden, J. S. *Organic Chemistry*, 3rd ed.; Brooks/Cole Publishing Co.: Monterey, CA, 1982.
- Beuermann, S.; Paquet, D. A., Jr.; McMinn, J. H.; Hutchinson, R. A. *Macromolecules* **1996**, *29*, 4206–4215.
- Pintauer, T.; Reinohl, U.; Feth, M.; Bertagnolli, H.; Matyjaszewski, K. *Eur. J. Inorg. Chem.* **2003**, *11*, 2082–2094.
- Kickelbick, G.; Pintauer, T.; Matyjaszewski, K. *New J. Chem.* **2002**, *26*, 462–468.
- Crabtree, R. H. *The Organometallic Chemistry of the Transition Metals*, 3rd ed.; John Wiley and Sons: New York, 2001.
- Queffelec, J.; Gaynor, S. G.; Matyjaszewski, K. *Macromolecules* **2000**, *33*, 8629–8639.
- Rubinstein, M.; Colby, R. H. *Polymer Physics*; Oxford University Press: New York, 2003.
- Flory, P. J. *Principles of Polymer Chemistry*; Cornell University Press: Ithaca, NY, 1953.
- Goldwasser, J. M.; Adolph, H. G. *Polym. Eng. Sci.* **1986**, *26*, 1510–1513.
- The PDI trend observed with [PMDETA]₀: [Cu(I)Br]₀ = 2:1 deviates from those seen at other ratios, but we believe this deviation is statistically insignificant. In the present report, we do not attempt any further clarification of this issue because it is largely irrelevant to the main point of this paper (as discussed later in the paragraph).

MA060374Y

Errata

p. 4683 left, line 24 from top: "5 orders" should be "4 orders".

p.4684 right, line 10 from top: "section 2.2" should be "section 2.3".

p.4689 right, line 39 from top: "Johnson III, R. D.; Release 12 (August 2005) ed." should be "Johnson III, R. D. *NIST Computational Chemistry Comparison and Benchmark Database*, Release 12 (August 2005); <http://srdata.nist.gov/cccbdb/>".

Supporting Information for

Inhibitive Chain Transfer to Ligand in the ATRP of *n*-Butyl Acrylate

Rahul Sharma, Ayush Goyal, James M. Caruthers, and You-Yeon Won*

School of Chemical Engineering, Purdue University, West Lafayette, Indiana 47907

* yywon@ecn.purdue.edu

Section 1: Kinetic balance equations for modeling the ATRP of nBA using the conventional ATRP mechanism.

$$\frac{d[\text{IBr}]}{dt} = k_d[\text{I}\bullet][\text{CuBr}_2] - k_a[\text{IBr}][\text{CuBr}]$$

$$\frac{d[\text{I}\bullet]}{dt} = -k_d[\text{I}\bullet][\text{CuBr}_2] + k_a[\text{IBr}][\text{CuBr}] - k_p[\text{I}\bullet][\text{M}] - \frac{1}{2}(k_{tc,1} + k_{tc})[\text{I}\bullet][\lambda_0] - k_{tc,1}[\text{I}\bullet]^2$$

$$\frac{d[\lambda_0]}{dt} = -k_d[\lambda_0][\text{CuBr}_2] + k_a[\mu_0][\text{CuBr}] + k_p[\text{I}\bullet][\text{M}] - \frac{1}{2}(k_{tc,1} + k_{tc})[\text{I}\bullet][\lambda_0] - k_{tc}[\lambda_0]^2$$

$$\frac{d[\lambda_1]}{dt} = -k_d[\lambda_1][\text{CuBr}_2] + k_a[\mu_1][\text{CuBr}] + k_p[\text{I}\bullet][\text{M}] - \frac{1}{2}(k_{tc,1} + k_{tc})[\text{I}\bullet][\lambda_1] - k_{tc}[\lambda_0][\lambda_1] + k_p[\lambda_0][\text{M}]$$

$$\frac{d[\lambda_2]}{dt} = -k_d[\lambda_2][\text{CuBr}_2] + k_a[\mu_2][\text{CuBr}] + k_p[\text{I}\bullet][\text{M}] - \frac{1}{2}(k_{tc,1} + k_{tc})[\text{I}\bullet][\lambda_2] - k_{tc}[\lambda_0][\lambda_2] + k_p[\lambda_0][\text{M}] + 2k_p[\lambda_1][\text{M}]$$

$$\frac{d[\mu_0]}{dt} = k_d[\lambda_0][\text{CuBr}_2] - k_a[\mu_0][\text{CuBr}]$$

$$\frac{d[\mu_1]}{dt} = k_d[\lambda_1][\text{CuBr}_2] - k_a[\mu_1][\text{CuBr}]$$

$$\frac{d[\mu_2]}{dt} = k_d[\lambda_2][\text{CuBr}_2] - k_a[\mu_2][\text{CuBr}]$$

$$\frac{d[\chi_0]}{dt} = \frac{1}{2}(k_{tc,1} + k_{tc})[\text{I}\bullet][\lambda_0] + \frac{k_{tc}}{2}[\lambda_0]^2$$

$$\frac{d[\chi_1]}{dt} = \frac{1}{2}(k_{tc,1} + k_{tc})[\text{I}\bullet][\lambda_1] + k_{tc}[\lambda_0][\lambda_1]$$

$$\frac{d[\chi_2]}{dt} = \frac{1}{2}(k_{tc,1} + k_{tc})[\text{I}\bullet][\lambda_2] + k_{tc}([\lambda_0][\lambda_2] + [\lambda_1]^2)$$

$$\frac{d[\text{CuBr}]}{dt} = k_d([\lambda_0] + [\text{I}\bullet])[\text{CuBr}_2] - k_a([\mu_0] + [\text{IBr}])[\text{CuBr}]$$

$$\frac{d[\text{M}]}{dt} = -k_p[\lambda_0][\text{M}] - k_p[\text{I}\bullet][\text{M}]$$

$$[\text{CuBr}] + [\text{CuBr}_2] = [\text{CuBr}]_0$$

$$[\lambda_i] = \sum_{n=1}^{\infty} n^i [\text{R}_n \bullet] \quad i = 1, 2, 3$$

$$[\mu_i] = \sum_{n=1}^{\infty} n^i [\text{R}_n \text{Br}] \quad i = 1, 2, 3$$

$$[\chi_i] = \sum_{n=1}^{\infty} n^i [\text{P}_n] \quad i = 1, 2, 3$$

$$k_{tc} = k_{tc0} DP^{-(0.065+0.016DP)}$$

$$DP = 113 + \frac{[M]_0}{[I]_0} x$$

$$x = 1 - \frac{[M]}{[M]_0}$$

$$k_{tc,1} = k_{tc} (x = 0)$$

Section 2: Kinetic balance equations for modeling the ATRP of nBA on the basis of the mechanism that accounts for the chain transfer to PMDETA.

$$\frac{d[IBr]}{dt} = k_d[I\bullet][CuBr_2] - k_a[IBr][CuBr]$$

$$\begin{aligned} \frac{d[I\bullet]}{dt} = & -k_d[I\bullet][CuBr_2] + k_a[IBr][CuBr] - k_p[I\bullet][M] - k_{tr}[I\bullet]([L] + [L^-]) - k_{ti}[I\bullet] \\ & ([L\bullet] + [L^-\bullet]) - \frac{1}{2}(k_{tc,1} + k_{tc})[I\bullet][\lambda_0] - k_{tc,1}[I\bullet]^2 \end{aligned}$$

$$\begin{aligned} \frac{d[\lambda_0]}{dt} = & -k_d[\lambda_0][CuBr_2] + k_a[\mu_0][CuBr] + k_p[I\bullet][M] - k_{tr}[\lambda_0]([L] + [L^-]) - k_{ti}[\lambda_0] \\ & ([L\bullet] + [L^-\bullet]) - \frac{1}{2}(k_{tc,1} + k_{tc})[I\bullet][\lambda_0] - k_{tc}[\lambda_0]^2 \end{aligned}$$

$$\begin{aligned} \frac{d[\lambda_1]}{dt} = & -k_d[\lambda_1][CuBr_2] + k_a[\mu_1][CuBr] + k_p[I\bullet][M] - k_{tr}[\lambda_1]([L] + [L^-]) - k_{ti}[\lambda_1] \\ & ([L\bullet] + [L^-\bullet]) - \frac{1}{2}(k_{tc,1} + k_{tc})[I\bullet][\lambda_1] - k_{tc}[\lambda_0][\lambda_1] + k_p[\lambda_0][M] \end{aligned}$$

$$\begin{aligned} \frac{d[\lambda_2]}{dt} = & -k_d[\lambda_2][CuBr_2] + k_a[\mu_2][CuBr] + k_p[I\bullet][M] - k_{tr}[\lambda_2]([L] + [L^-]) - k_{ti}[\lambda_2] \\ & ([L\bullet] + [L^-\bullet]) - \frac{1}{2}(k_{tc,1} + k_{tc})[I\bullet][\lambda_2] - k_{tc}[\lambda_0][\lambda_2] + k_p[\lambda_0][M] + 2k_p[\lambda_1][M] \end{aligned}$$

$$\frac{d[\mu_0]}{dt} = k_d[\lambda_0][CuBr_2] - k_a[\mu_0][CuBr]$$

$$\frac{d[\mu_1]}{dt} = k_d[\lambda_1][CuBr_2] - k_a[\mu_1][CuBr]$$

$$\frac{d[\mu_2]}{dt} = k_d[\lambda_2][CuBr_2] - k_a[\mu_2][CuBr]$$

$$\frac{d[\chi_0]}{dt} = k_{tr}[\lambda_0]([L] + [L^-]) + k_{ti}[\lambda_0]([L\bullet] + [L^-\bullet]) + \frac{1}{2}(k_{tc,1} + k_{tc})[I\bullet][\lambda_0] + \frac{k_{tc}}{2}[\lambda_0]^2$$

$$\frac{d[\chi_1]}{dt} = k_{tr}[\lambda_1]([L] + [L^-]) + k_{ti}[\lambda_1]([L\bullet] + [L^-\bullet]) + \frac{1}{2}(k_{tc,1} + k_{tc})[I\bullet][\lambda_1] + k_{tc}[\lambda_0][\lambda_1]$$

$$\frac{d[\chi_2]}{dt} = k_{tr}[\lambda_2]([L] + [L^-]) + k_{ti}[\lambda_2]([L\bullet] + [L^-\bullet]) + \frac{1}{2}(k_{tc,1} + k_{tc})[I\bullet][\lambda_2] + k_{tc}([\lambda_0][\lambda_2] + [\lambda_1]^2)$$

$$\frac{d[CuBr]}{dt} = k_d([\lambda_0] + [I\bullet])[CuBr_2] - k_a([\mu_0] + [IBr])[CuBr]$$

$$\frac{d[M]}{dt} = -k_p[\lambda_0][M] - k_p[I\bullet][M]$$

$$\frac{d[L]}{dt} = -k_{tr}([\lambda_0] + [I\bullet])[L] + k_{ti}([\lambda_0] + [I\bullet])[L\bullet] + k_{ti}[L\bullet]([L\bullet] + [L^-\bullet])$$

$$\frac{d[L\bullet]}{dt} = k_{tr}([\lambda_0] + [I\bullet])[L] - k_{ti}([\lambda_0] + [I\bullet])[L\bullet] - k_{ti}[L\bullet](2[L\bullet] + [L^-\bullet])$$

$$\frac{d[L^-]}{dt} = -k_{tr}([\lambda_0] + [I\bullet])[L^-] + k_{ti}([\lambda_0] + [I\bullet])[L^-\bullet] + k_{ti}[L\bullet]([L\bullet] + [L^-\bullet]) + k_{ti}[L^-\bullet]^2$$

$$\frac{d[L^-\bullet]}{dt} = k_{tr}([\lambda_0] + [I\bullet])[L^-] - k_{ti}([\lambda_0] + [I\bullet])[L^-\bullet] - k_{ti}[L^-\bullet]([L\bullet] + [L^-\bullet])$$

$$\frac{d[L^-\bullet]}{dt} = k_{ti}\left(\frac{1}{2}[L\bullet] + [L^-\bullet]\right)[L^-\bullet]$$

Section 3: Kinetic balance equations for modeling the ATRP of nBA on the basis of the proposed ATRP mechanism that includes the chain transfer to ligand and the difference in reactivity between the free and copper-bound ligand species.

$$\frac{d[IBr]}{dt} = k_d[I\bullet][CuBr_2] - k_a[IBr][CuBr]$$

$$\begin{aligned} \frac{d[I\bullet]}{dt} = & -k_d[I\bullet][CuBr_2] + k_a[IBr][CuBr] - k_p[I\bullet][M] - k'_{tr}[I\bullet]([CuL] + [CuL^-]) - k_{tr}[I\bullet] \\ & ([L] + [L^-]) - k'_{ti}[I\bullet]([CuL\bullet] + [CuL^-\bullet]) - k_{ti}[I\bullet]([L\bullet] + [L^-\bullet]) - \frac{1}{2}(k_{tc,1} + k_{tc})[I\bullet][\lambda_0] - \\ & k_{tc,1}[I\bullet]^2 \end{aligned}$$

$$\begin{aligned} \frac{d[\lambda_0]}{dt} = & -k_d[\lambda_0][CuBr_2] + k_a[\mu_0][CuBr] + k_p[I\bullet][M] - k'_{tr}[\lambda_0]([CuL] + [CuL^-]) - k_{tr}[\lambda_0] \\ & ([L] + [L^-]) - k'_{ti}[\lambda_0]([CuL\bullet] + [CuL^-\bullet]) - k_{ti}[\lambda_0]([L\bullet] + [L^-\bullet]) - \frac{1}{2}(k_{tc,1} + k_{tc})[I\bullet][\lambda_0] - \\ & k_{tc}[\lambda_0]^2 \end{aligned}$$

$$\begin{aligned} \frac{d[\lambda_1]}{dt} = & -k_d[\lambda_1][CuBr_2] + k_a[\mu_1][CuBr] + k_p[I\bullet][M] - k'_{tr}[\lambda_1]([CuL] + [CuL^-]) - k_{tr}[\lambda_1] \\ & ([L] + [L^-]) - k'_{ti}[\lambda_1]([CuL\bullet] + [CuL^-\bullet]) - k_{ti}[\lambda_1]([L\bullet] + [L^-\bullet]) - \frac{1}{2}(k_{tc,1} + k_{tc})[I\bullet][\lambda_1] - \\ & k_{tc}[\lambda_0][\lambda_1] + k_p[\lambda_0][M] \end{aligned}$$

$$\begin{aligned} \frac{d[\lambda_2]}{dt} &= -k_d[\lambda_2][\text{CuBr}_2] + k_a[\mu_2][\text{CuBr}] + k_p[\text{I}\bullet][\text{M}] - k'_{tr}[\lambda_2]([\text{CuL}] + [\text{CuL}^-]) - k_{tr}[\lambda_2] \\ &\quad ([\text{L}] + [\text{L}^-]) - k'_{ti}[\lambda_2]([\text{CuL}\bullet] + [\text{CuL}^-\bullet]) - k_{ti}[\lambda_2]([\text{L}\bullet] + [\text{L}^-\bullet]) - \frac{1}{2}(k_{tc,i} + k_{tc})[\text{I}\bullet][\lambda_2] - \\ &\quad k_{tc}[\lambda_0][\lambda_2] + k_p[\lambda_0][\text{M}] + 2k_p[\lambda_1][\text{M}] \end{aligned}$$

$$\frac{d[\mu_0]}{dt} = k_d[\lambda_0][\text{CuBr}_2] - k_a[\mu_0][\text{CuBr}]$$

$$\frac{d[\mu_1]}{dt} = k_d[\lambda_1][\text{CuBr}_2] - k_a[\mu_1][\text{CuBr}]$$

$$\frac{d[\mu_2]}{dt} = k_d[\lambda_2][\text{CuBr}_2] - k_a[\mu_2][\text{CuBr}]$$

$$\begin{aligned} \frac{d[\chi_0]}{dt} &= k'_{tr}[\lambda_0]([\text{CuL}] + [\text{CuL}^-]) + k_{tr}[\lambda_0]([\text{L}] + [\text{L}^-]) + k'_{ti}[\lambda_0]([\text{CuL}\bullet] + [\text{CuL}^-\bullet]) + k_{ti}[\lambda_0] \\ &\quad ([\text{L}\bullet] + [\text{L}^-\bullet]) + \frac{1}{2}(k_{tc,i} + k_{tc})[\text{I}\bullet][\lambda_0] + \frac{k_{tc}}{2}[\lambda_0]^2 \end{aligned}$$

$$\begin{aligned} \frac{d[\chi_1]}{dt} &= k'_{tr}[\lambda_1]([\text{CuL}] + [\text{CuL}^-]) + k_{tr}[\lambda_1]([\text{L}] + [\text{L}^-]) + k'_{ti}[\lambda_1]([\text{CuL}\bullet] + [\text{CuL}^-\bullet]) + k_{ti}[\lambda_1] \\ &\quad ([\text{L}\bullet] + [\text{L}^-\bullet]) + \frac{1}{2}(k_{tc,i} + k_{tc})[\text{I}\bullet][\lambda_1] + k_{tc}[\lambda_0][\lambda_1] \end{aligned}$$

$$\begin{aligned} \frac{d[\chi_2]}{dt} &= k'_{tr}[\lambda_2]([\text{CuL}] + [\text{CuL}^-]) + k_{tr}[\lambda_2]([\text{L}] + [\text{L}^-]) + k'_{ti}[\lambda_2]([\text{CuL}\bullet] + [\text{CuL}^-\bullet]) + k_{ti}[\lambda_2] \\ &\quad ([\text{L}\bullet] + [\text{L}^-\bullet]) + \frac{1}{2}(k_{tc,i} + k_{tc})[\text{I}\bullet][\lambda_2] + k_{tc}([\lambda_0][\lambda_2] + [\lambda_1]^2) \end{aligned}$$

$$\frac{d[\text{CuBr}]}{dt} = k_d([\lambda_0] + [\text{I}\bullet])[\text{CuBr}_2] - k_a([\mu_0] + [\text{I}\text{Br}])[\text{CuBr}]$$

$$\frac{d[\text{M}]}{dt} = -k_p[\lambda_0][\text{M}] - k_p[\text{I}\bullet][\text{M}]$$

$$\begin{aligned} \frac{d[\text{CuL}]}{dt} &= -k'_{tr}([\lambda_0] + [\text{I}\bullet])[\text{CuL}] + k'_{ti}([\lambda_0] + [\text{I}\bullet])[\text{CuL}\bullet] + k'_{ti}[\text{CuL}\bullet]([\text{CuL}\bullet] + \frac{1}{2}[\text{CuL}^-\bullet]) \\ &\quad + \frac{1}{2}k''_{ti}[\text{CuL}\bullet]([\text{L}\bullet] + [\text{L}^-\bullet]) \end{aligned}$$

$$\begin{aligned} \frac{d[\text{L}]}{dt} &= -k_{tr}([\lambda_0] + [\text{I}\bullet])[\text{L}] + k_{ti}([\lambda_0] + [\text{I}\bullet])[\text{L}\bullet] + k_{ti}[\text{L}\bullet]([\text{L}\bullet] + \frac{1}{2}[\text{L}^-\bullet]) + \frac{1}{2}k''_{ti}[\text{L}\bullet] \\ &\quad ([\text{CuL}\bullet] + [\text{CuL}^-\bullet]) \end{aligned}$$

$$\begin{aligned} \frac{d[\text{CuL}\bullet]}{dt} &= k'_{tr}([\lambda_0] + [\text{I}\bullet])[\text{CuL}] - k'_{ti}([\lambda_0] + [\text{I}\bullet])[\text{CuL}\bullet] - k'_{ti}[\text{CuL}\bullet](2[\text{CuL}\bullet] + [\text{CuL}^-\bullet]) \\ &\quad - k''_{ti}[\text{CuL}\bullet]([\text{L}\bullet] + [\text{L}^-\bullet]) \end{aligned}$$

$$\begin{aligned} \frac{d[\text{L}\bullet]}{dt} &= k_{tr}([\lambda_0] + [\text{I}\bullet])[\text{L}] - k_{ti}([\lambda_0] + [\text{I}\bullet])[\text{L}\bullet] - k_{ti}[\text{L}\bullet](2[\text{L}\bullet] + [\text{L}^-\bullet]) - k''_{ti}[\text{L}\bullet]([\text{CuL}\bullet] \\ &\quad + [\text{L}^-\bullet]) \end{aligned}$$

$$\begin{aligned} \frac{d[\text{CuL}^-]}{dt} = & -k'_{\text{tr}}([\lambda_0] + [\text{I}\bullet])[\text{CuL}^-] + k'_{\text{ti}}([\lambda_0] + [\text{I}\bullet])[\text{CuL}^-\bullet] + k'_{\text{ui}}[\text{CuL}\bullet]([\text{CuL}\bullet] + [\text{CuL}^-\bullet]) \\ & + k'_{\text{ui}}[\text{CuL}^-\bullet]^2 + \frac{1}{2}k''_{\text{ui}}[\text{CuL}\bullet]([\text{L}\bullet] + [\text{L}^-\bullet]) + \frac{1}{2}k''_{\text{ui}}[\text{L}\bullet][\text{CuL}^-\bullet] + \frac{1}{2}k''_{\text{ui}}[\text{CuL}^-\bullet] \\ & [\text{L}^-\bullet] \end{aligned}$$

$$\begin{aligned} \frac{d[\text{L}^-]}{dt} = & -k_{\text{tr}}([\lambda_0] + [\text{I}\bullet])[\text{L}^-] + k_{\text{ti}}([\lambda_0] + [\text{I}\bullet])[\text{L}^-\bullet] + k_{\text{ui}}[\text{L}\bullet]([\text{L}\bullet] + [\text{L}^-\bullet]) + k_{\text{ui}}[\text{L}^-\bullet]^2 + \frac{1}{2} \\ & k''_{\text{ui}}[\text{L}\bullet]([\text{CuL}\bullet] + [\text{CuL}^-\bullet]) + \frac{1}{2}k''_{\text{ui}}[\text{CuL}\bullet][\text{L}^-\bullet] + \frac{1}{2}k''_{\text{ui}}[\text{L}^-\bullet][\text{CuL}^-\bullet] \end{aligned}$$

$$\begin{aligned} \frac{d[\text{CuL}^-\bullet]}{dt} = & k'_{\text{tr}}([\lambda_0] + [\text{I}\bullet])[\text{CuL}^-] - k'_{\text{ti}}([\lambda_0] + [\text{I}\bullet])[\text{CuL}^-\bullet] - k'_{\text{ui}}[\text{CuL}^-\bullet]([\text{CuL}\bullet] + [\text{CuL}^-\bullet]) \\ & - k''_{\text{ui}}[\text{L}^-\bullet]([\text{CuL}\bullet] + [\text{CuL}^-\bullet]) \end{aligned}$$

$$\begin{aligned} \frac{d[\text{L}^-\bullet]}{dt} = & k_{\text{tr}}([\lambda_0] + [\text{I}\bullet])[\text{L}^-] - k_{\text{ti}}([\lambda_0] + [\text{I}\bullet])[\text{L}^-\bullet] - k_{\text{ui}}[\text{L}^-\bullet]([\text{L}\bullet] + [\text{L}^-\bullet]) - k''_{\text{ui}}[\text{CuL}^-\bullet] \\ & ([\text{L}\bullet] + [\text{L}^-\bullet]) \end{aligned}$$

$$\frac{d[\text{CuL}^-\bullet]}{dt} = k'_{\text{ui}}\left(\frac{1}{2}[\text{CuL}\bullet] + [\text{CuL}^-\bullet]\right)[\text{CuL}^-\bullet] + \frac{1}{2}k''_{\text{ui}}[\text{CuL}^-\bullet]([\text{L}\bullet] + [\text{L}^-\bullet])$$

$$\frac{d[\text{L}^-\bullet]}{dt} = k_{\text{ui}}\left(\frac{1}{2}[\text{L}\bullet] + [\text{L}^-\bullet]\right)[\text{L}^-\bullet] + \frac{1}{2}k''_{\text{ui}}[\text{L}^-\bullet]([\text{CuL}\bullet] + [\text{CuL}^-\bullet])$$

$$k'_{\text{tr}} = \frac{k_{\text{tr}}}{\alpha}$$

$$k'_{\text{ti}} = \alpha k_{\text{ti}}$$

$$k'_{\text{ui}} = \alpha^2 k_{\text{ui}}$$

$$k''_{\text{ui}} = \alpha k_{\text{ui}}$$

Section 4: Procedures for calculating the absolute PDI values for the PEO-PnBA product.

The time-dependent molecular weight distribution of the ATRP product (i.e., PEO-PnBA diblock copolymer) can be considered in terms of the populations of chains of all possible compositions for a given overall chain length n at time t :

$$p_{\text{PEO-PnBA}}(n, t) = (1 - \beta(t)) \sum_{n_{\text{PEO}}=1}^{n-1} p_{\text{PEO}}(n_{\text{PEO}}) p_{\text{PnBA}}(n - n_{\text{PEO}}, t) + \beta(t) p_{\text{PEO}}(n)$$

where $p_{\text{PEO-PnBA}}(n, t)$, $p_{\text{PEO}}(n)$, and $p_{\text{PnBA}}(n, t)$ are the number fractions of chains of length n within the individual categories of PEO-PnBA, PEO and PnBA, respectively, and β is defined as $\beta \equiv ([\text{IBr}] + [\text{I}\bullet] + [\text{P}_0]) / ([\text{IBr}] + [\text{I}\bullet] + [\text{P}_0] + [\lambda_0] + [\mu_0] + [\chi_0])$. Starting from this expression, it is not difficult to show that the zeroth, first and second moments

($\mu_0^{\text{PEO-PnBA}}$, $\mu_1^{\text{PEO-PnBA}}$ and $\mu_2^{\text{PEO-PnBA}}$, respectively) of the distribution $p_{\text{PEO-PnBA}}(n, t)$ at time t can be written as:

$$\begin{aligned}\mu_0^{\text{PEO-PnBA}} &= (1-\beta)\mu_0^{\text{PEO}}\mu_0^{\text{PnBA}} + \beta\mu_0^{\text{PEO}}; \\ \mu_1^{\text{PEO-PnBA}} &= (1-\beta)(\mu_0^{\text{PEO}}\mu_1^{\text{PnBA}} + \mu_1^{\text{PEO}}\mu_0^{\text{PnBA}}) + \beta\mu_1^{\text{PEO}}; \\ \mu_2^{\text{PEO-PnBA}} &= (1-\beta)(\mu_0^{\text{PEO}}\mu_2^{\text{PnBA}} + 2\mu_1^{\text{PEO}}\mu_1^{\text{PnBA}} + \mu_2^{\text{PEO}}\mu_0^{\text{PnBA}}) + \beta\mu_2^{\text{PEO}}.\end{aligned}$$

Once the diblock moments are known, the number- and weight-average degrees of polymerization and the PDI for the PEO-PnBA product can be evaluated using:

$$\begin{aligned}\overline{\text{DP}}_n^{\text{PEO-PnBA}} &= \frac{\mu_1^{\text{PEO-PnBA}}}{\mu_0^{\text{PEO-PnBA}}}; \\ \overline{\text{DP}}_w^{\text{PEO-PnBA}} &= \frac{\mu_2^{\text{PEO-PnBA}}}{\mu_1^{\text{PEO-PnBA}}}; \\ \text{PDI} &= \frac{\overline{\text{DP}}_w^{\text{PEO-PnBA}}}{\overline{\text{DP}}_n^{\text{PEO-PnBA}}}.\end{aligned}$$

In this work, the zeroth, first and second moments of the molecular weight distributions for the individual blocks (i.e., μ_i^{PEO} and μ_i^{PnBA} with $i = 0, 1, 2$) were computed from estimates of $p_{\text{PEO}}(n)$ and $p_{\text{PBA}}(n, t)$ using the continuum approximation as described below.

The PEO-block distribution $p_{\text{PEO}}(n)$ was estimated from the GPC trace of the PEO macroinitiator; the experimental GPC data were fit to the model

$$p_{\text{PEO}}(n) = \frac{w}{\sqrt{2\pi\sigma_1}} e^{-\frac{(n-\bar{n}_1)^2}{2\sigma_1^2}} + \frac{(1-w)}{\sqrt{2\pi\sigma_2}} e^{-\frac{(n-\bar{n}_2)^2}{2\sigma_2^2}}.$$

Here the use of two Gaussian distribution functions was necessitated by the reproducible occurrence of a small shoulder at the high molecular weight side of the GPC profile.

In doing the above analysis, the PEO molecular weights determined by GPC on the basis of polystyrene standard samples were converted into absolute molecular weight values using the following relation

$$M_{\text{PEO}} = \left(\frac{K_{\text{PS}}}{K_{\text{PEO}}} M_{\text{PS}}^{(1+\alpha_{\text{PS}})} \right)^{\frac{1}{(1+\alpha_{\text{PEO}})}}$$

where K_x and α_x are the Mark-Houwink prefactor and exponent, respectively, for polymer of type x in THF.

Assuming that the chain length distribution of the PnBA block also follows a Gaussian distribution, $p_{\text{PBA}}(n, t)$ can be written as

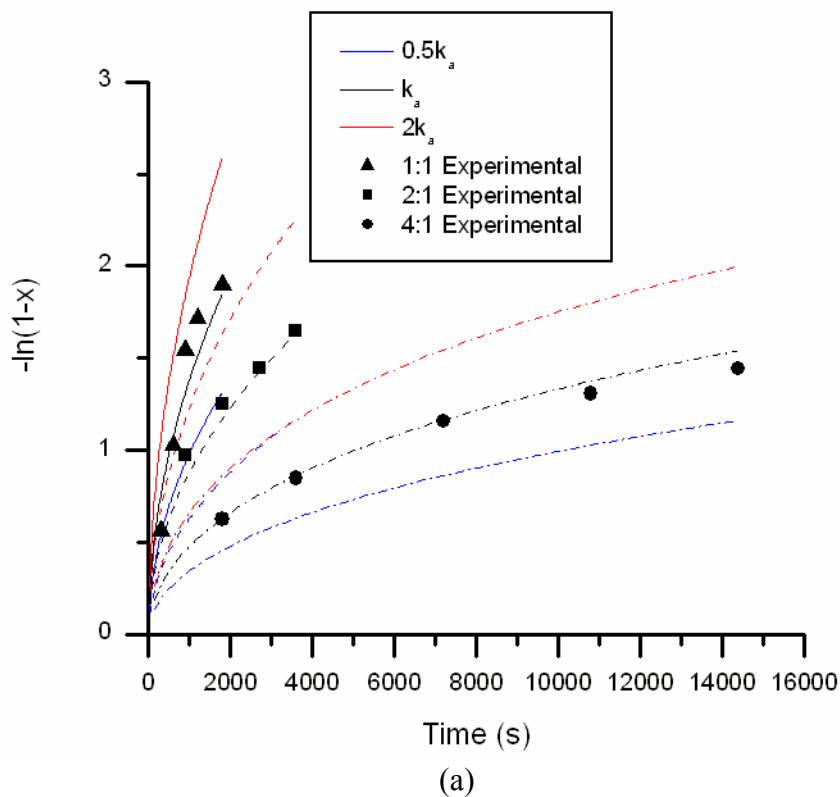
$$p_{\text{PBA}}(n, t) = \frac{1}{\sqrt{2\pi\sigma}} e^{-\frac{(n-\bar{n})^2}{2\sigma^2}}.$$

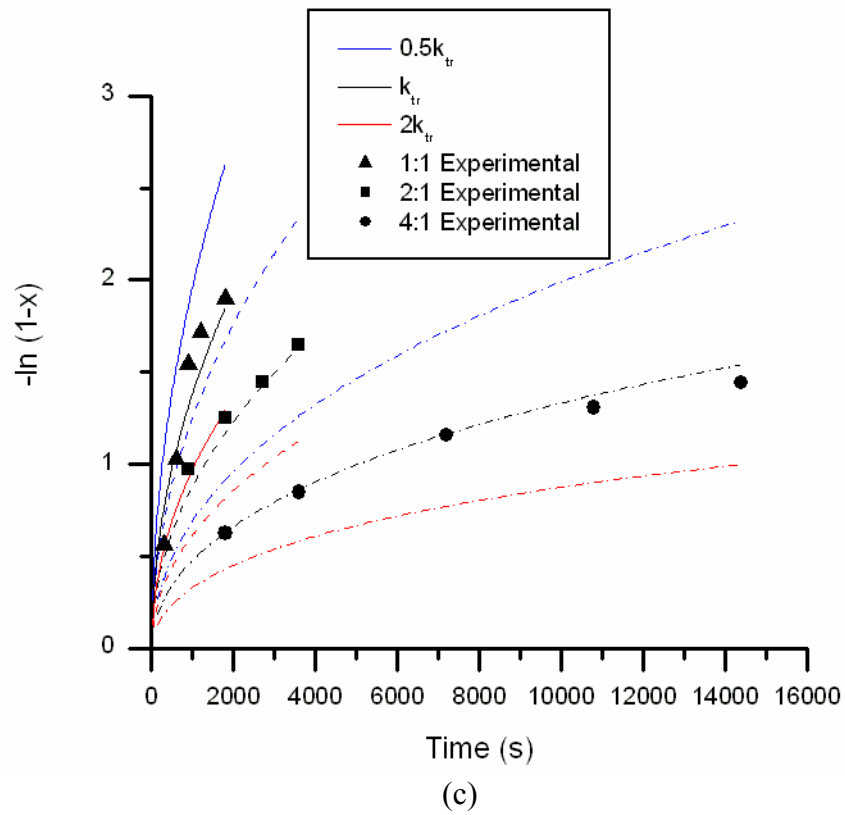
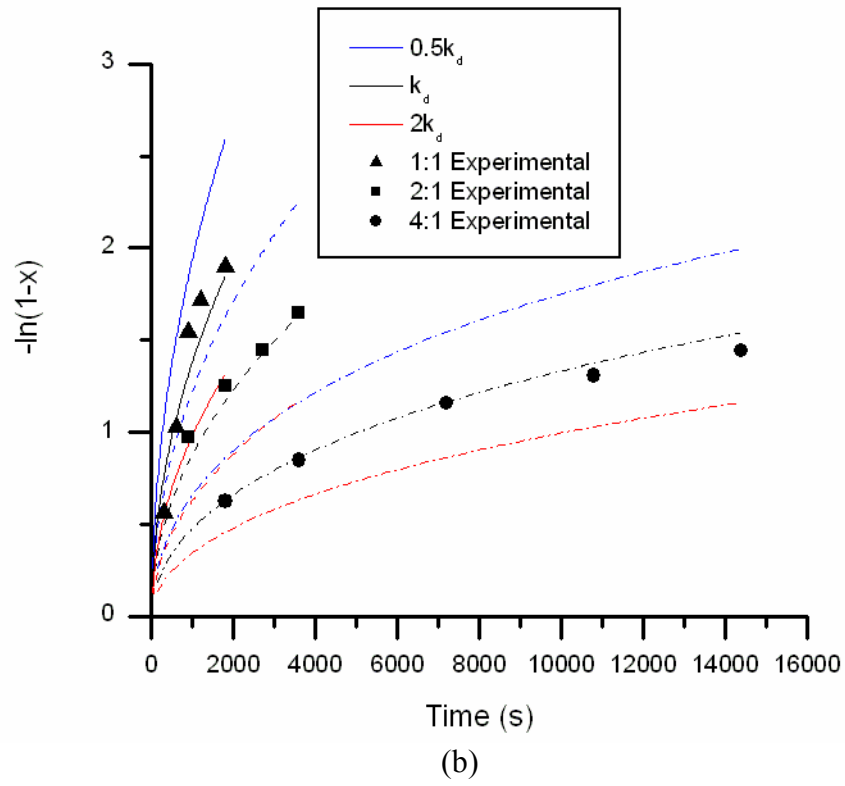
The mean $\bar{n}(t)$ and the standard deviation $\sigma(t)$ of this distribution can be evaluated from the kinetic modeling results:

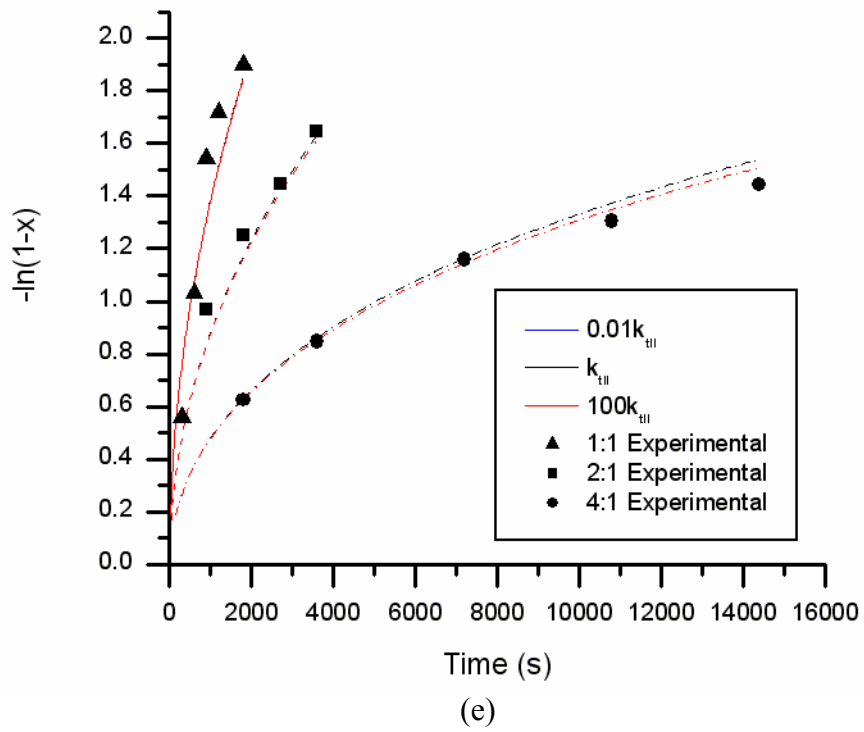
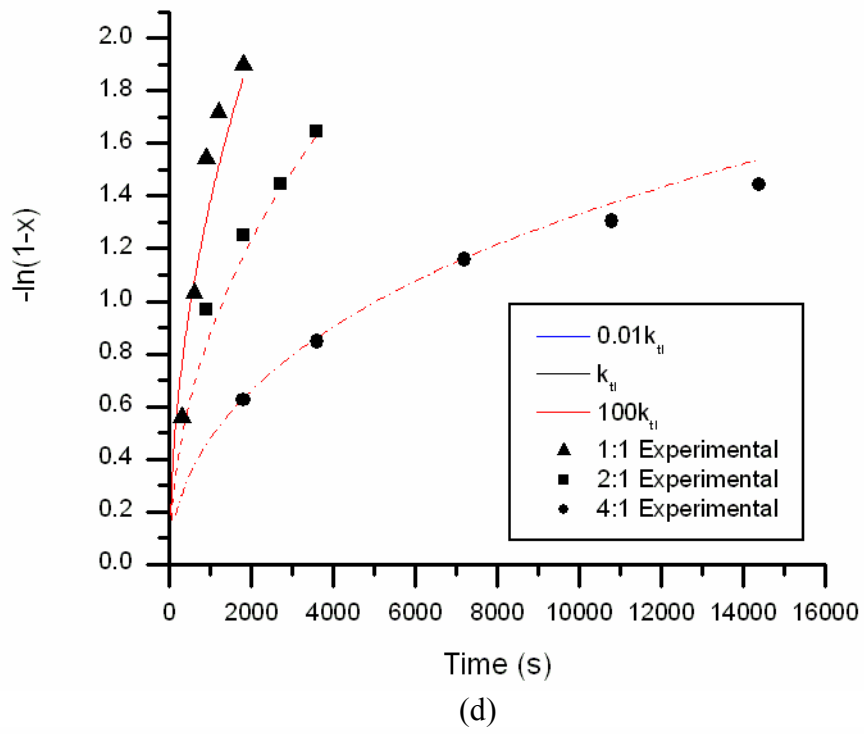
$$\bar{n}(t) = \frac{[\lambda_1] + [\mu_1] + [\chi_1]}{[\lambda_0] + [\mu_0] + [\chi_0]},$$

$$\sigma(t) = \sqrt{\frac{[\lambda_2] + [\mu_2] + [\chi_2]}{[\lambda_0] + [\mu_0] + [\chi_0]} - \bar{n}(t)^2}.$$

Section 5: Sensitivity of the predictions of the proposed ATRP model to variations in the kinetic parameters (see Figures S1 (a) through (f) below).







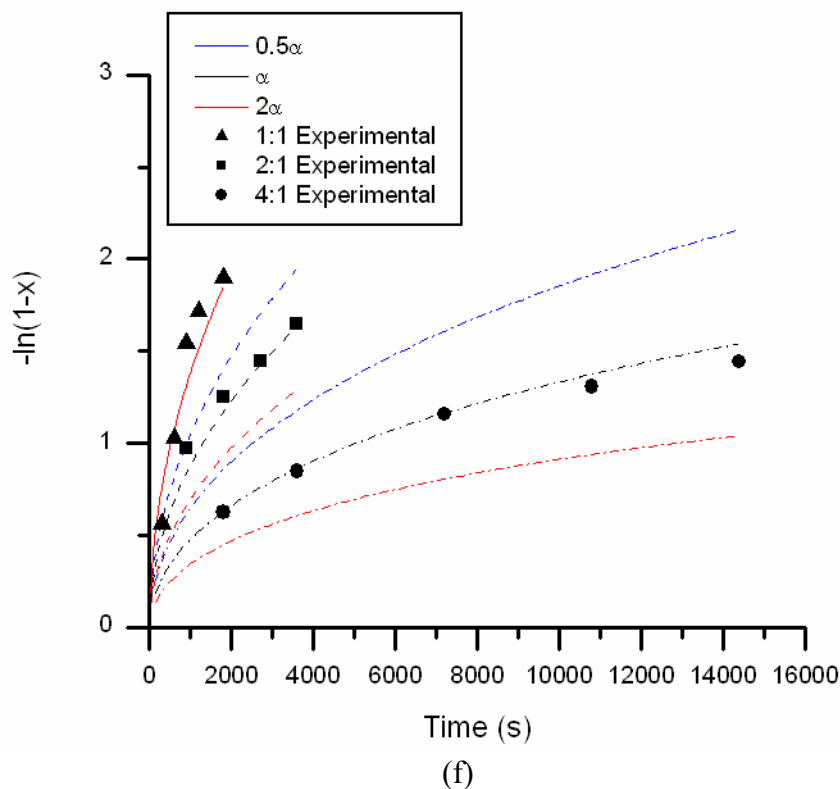
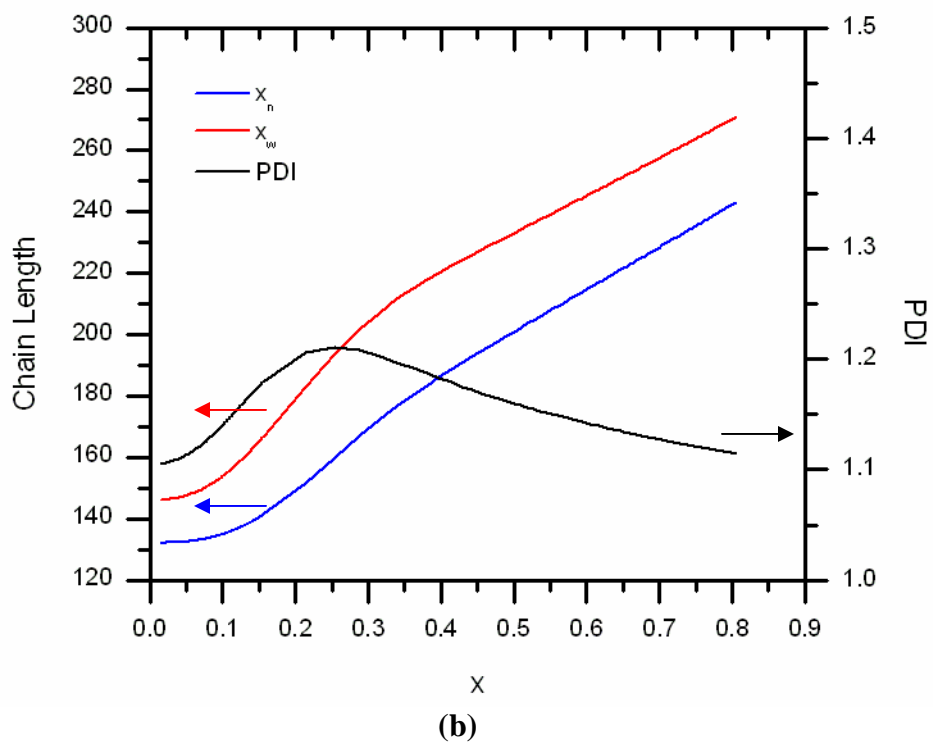
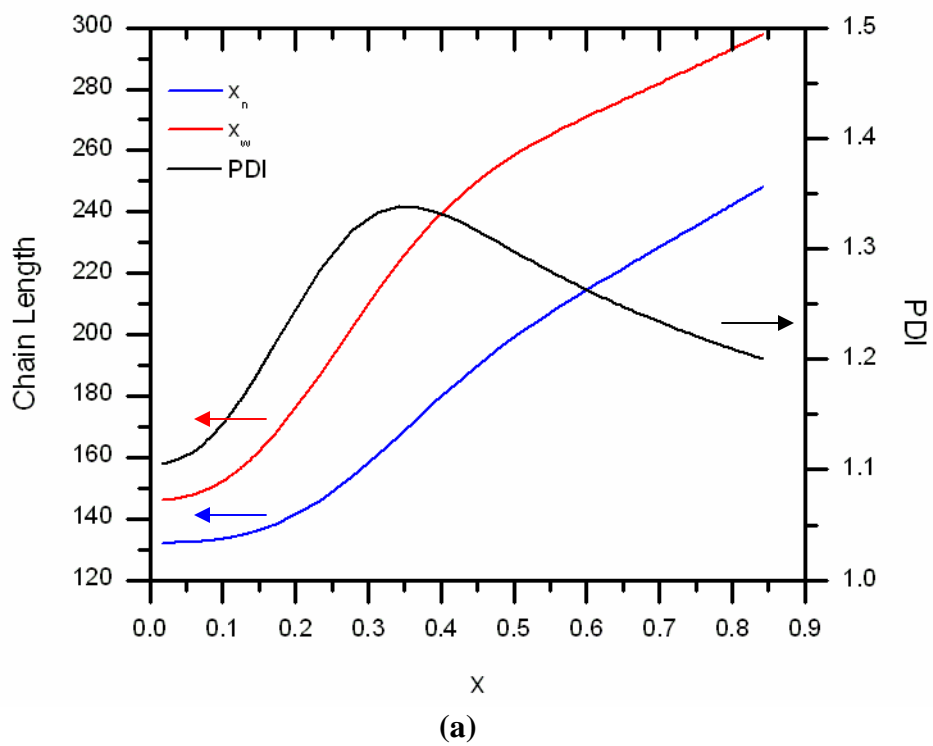


Figure S1. Demonstrations of how a factor of ten increase or decrease of the parameters (a) k_a , (b) k_d , (c) k_{tr} , (d) k_{tl} , (e) k_{tl} and (f) α from their best-fit values (Table 4) influences the predictions of the proposed ATRP model described in Section 3 of Supporting Information. The measured data points are same as in Figures 3 and 4 in the main text. Here, the solid, dashed and dashed-broken curves represent the ligand-to-copper ratios of $[PMDETA]_0:[Cu(I)Br]_0 = 1:1, 2:1$ and $4:1$, respectively. x denotes the monomer conversion.

Section 6: Predictions of the proposed ATRP model (Section 3 of Supporting Information) for the number-average and weight-average chain lengths (x_n and x_w , respectively) and polydispersity index (PDI) for the PEO-PnBA product as functions of the monomer conversion (x).



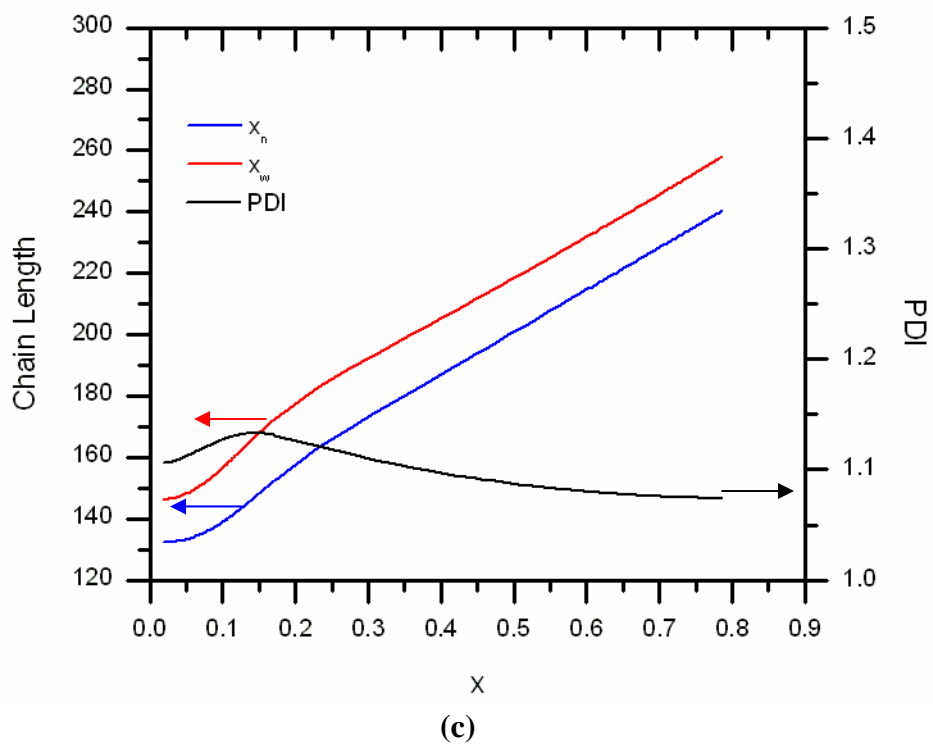


Figure S2. Evolution of cumulative chain lengths (i.e., x_n and x_w) and polydispersity (PDI) for the ATRP of nBA using the PEO macroinitiator. Here, model predictions are shown for the three different ligand-to-catalyst ratios of $[\text{PMDETA}]_0:[\text{Cu(I)Br}]_0 =$ (a) 1:1, (b) 2:1, and (c) 4:1.